

Modelling and Control of Dish-Stirling Solar/Gas Hybrid System



Edvin Wallander

Division of Industrial Electrical Engineering and Automation
Faculty of Engineering, Lund University

Modelling and Control of Dish-Stirling Solar/Gas Hybrid System

Master of Science

in

Engineering

by

Edvin Wallander



Division of Industrial Electrical Engineering and Automation

Department of Biomedical Engineering

Faculty of Engineering, LTH, Lund University

Examiner:
Mats Alaküla

Supervisors:
Francisco J. Márquez-Fernández (LTH)
Lars Larsson & Lars Olsson (Stirlingversal)

MARCH 2021

Summary

A Dish-Stirling system is a concentrated solar power generation system that has high conversion efficiency and produces warm water as well as electricity. The technology has received little attention the last 10 years due to the falling prices of solar panels. The company Stirlingversal has identified a need for flexibility and reliability in the future energy system and has developed a unique Dish-Stirling system to fill this role. In this thesis a model of the new system is developed and several different modes of operation are proposed and analysed. Two different generator types are modeled and tested with the Dish-Stirling system in order to examine if there is an optimal system configuration. The results are then used to simulate two potential implementations of the Dish-Stirling system at two different locations: Lund, Sweden and Johannesburg, South Africa. The systems are compared to a photovoltaic and battery based system that is of equivalent performance.

Sammanfattning

Ett Dish-Stirling system är ett kraftverk som använder koncentrerad solinstrålning. Systemet har en hög effektivitet och producerar både el och värme. Teknologin har fått lite uppmärksamhet de senaste 10 åren på grund av de sjunkande priserna för solpaneler. Företaget Stirlingversal har identifierat ett behov av flexibilitet och pålitlighet i det framtida energisystemet och har därav utvecklat ett unikt Dish-Stirling system som kan fylla den rollen. I det här arbetet utvecklas en modell av det nya systemet och flera olika systemkonfigurationer analyseras. Två olika generatorer modelleras för att undersöka om det finns en optimalt konfiguration. Resultatet används sedan för att studera två potentiella konfigurationer i två olika delar av världen: Lund, Sverige och Johannesburg, Sydafrika. Systemen jämförs med ett system som är baserat på solpaneler och batterier med ekvivalent prestanda.

ACKNOWLEDGEMENT

This thesis was done with the company Stirlingversal and the Division of Industrial Electrical Engineering and Automation at the Faculty of Engineering, LTH, at Lund University. The experience has been very rewarding thanks to the people involved. I would like to give a huge thanks to my supervisor Francisco J. Márquez-Fernández who has been very generous with his time and has been an invaluable resource for the process of this work. Both in terms of inspiration and ideas but also in my deeper understanding of the theory presented in this work.

I am also very grateful to Lars Larsson at Stirlingversal who has supported me and shown great confidence in my work and abilities. He has made this thesis possible and I am happy to get to be part of the development of this unique system. Lastly I would like to thank Lars Olsson that has volunteered much time and knowledge in order to help me along my way.

TABLE OF CONTENTS

1	Introduction	1
2	Background	3
2.1	Stirling System History	3
2.2	Dish-Stirling System	3
2.3	Photovoltaic systems	6
2.4	Power Converters	6
2.5	Power Quality	7
2.6	Generators	9
2.7	Conversion Topologies	10
2.8	Energy Storage	11
2.9	Electrolysis	12
2.10	Distributed Generation & Local Networks	14
3	Dish-Stirling Model	15
3.1	Receiver	15
3.2	Engine	18
4	Electrical Models	21
4.1	Induction Generator Mathematical Model	21
4.2	DFIG Control system	24
4.3	Speed Control Scheme	29
4.4	Hybrid Control	30
4.5	APF control	30
4.6	Electrolyser Model	31
5	Results	33
5.1	System Performance	33
5.2	Power Quality & Power Flow	35
5.3	Electrolyser Result	37
6	Energy System Comparison	39
6.1	System Definition	39
7	Conclusions and Future Work	50
A	Electrolyzer Equations	55

List of Figures

1.1	Image of the Stirlingversal Stirling-dish system and its functional parts	2
2.1	Theoretic Stirling eric and otto cycle [13]	5
2.2	Stirling engine pistons arranged in the Siemens arrangement [13]	6
2.3	SCIG system topology	10
2.4	DFIG system topology	11
2.5	Alkaline electrolyser [26]	13
3.1	Overview of Dish-Stirling model	15
3.2	Efficiency correlated to pressure, the line represents the $\gamma_e(\Delta p)$ polynomial	20
4.1	Equivalent circuit representation of the induction machine	21
4.2	Rotor-side control system	26
4.3	Equivalent circuit representation of RL filter connecting the GSC to the grid	27
4.4	Grid-side control system	28
4.5	Flowchart of temperature and speed control system	29
4.6	Configuration of SCIG with APF	31
4.7	DFIG system with electrolyser	32
4.8	SCIG system with APF and electrolyser	32
5.1	Model power output compared to real values	33
5.2	System output power and efficiency	34
5.3	System pressure and rotor speed performance	34
5.4	Fuel consumption at 30kW output power compared to irradiance	35
5.5	Reactive power with and without PQI	36
5.6	Converter power flow, reactive power compensation	36
5.7	Model IV graph and reference IV graph [33]	37
5.8	Converter power flow with electrolyser	37
6.1	Visual representation of the systems considered in the comparison	39
6.2	Average in-plane GHI profile PV power output, Lund	41
6.3	Average DNI profile and Dish-Stirling power generation, Lund	42
6.4	Energy mix and gas consumption, 33 unit systems, Lund	43
6.5	Energy mix and gas consumption, 99 unit system, Lund	43
6.6	Energy output over one year 33 units, Lund. A similar result is found for the 99 unit system	44
6.7	Project system cost over 20 years, Lund. Three gas costs are considered: c1, c2, c3 which can be seen in table 6.2	45
6.8	Average DNI profile and Dish-Stirling power output, Johannesburg	47
6.9	Energy mix and gas consumption, 33 unit system, Johannesburg	47

6.10	Energy mix and gas consumption, 99 unit system, Johannesburg	48
6.11	Total produced energy over one year, Johannesburg	48
6.12	Project system cost over 20 years, Johannesburg. Three gas costs are considered: c1, c2, c3 which can be seen in table 6.2	49
A.1	Static-Dynamic model of alkaline electrolyser [33]	56

List of Tables

3.1	System energy loss	16
3.2	Pressure difference values and engine efficiency at different irradiation values	19
4.1	Generator parameters	22
6.1	Lund PV system specifications	41
6.2	Cost values used in the comparison of PV and Dish-Stirling systems . . .	44
6.3	Cost Dish-Stirling systems in Lund	45
6.4	Specific costs of PV system in Lund	46
6.5	Johannesburg PV system specifications	46
6.6	Cost Dish-Stirling systems Johannesburg	49
6.7	Specific costs for PV system Johannesburg	49

List of Acronyms

DNI - Direct normal irradiation
GHI - Global horizontal irradiation
PV - Photovoltaic
DFIG - Doubly-fed induction generator
SCIG - Squirrel cage induction generator
PMSG - Permanent magnet synchronous generator
SG - Synchronous generator
SM - Synchronous machine
AM - Asynchronous machine
rmf - Rotating magnetic field
CSP - Concentrated solar power
PCU - Power conversion unit
NOX - Nitrogen oxides
WECS - Wind energy conversion systems
GHG - Greenhouse gas
DC - Direct current
AC - Alternating current
GSC - Grid-side convert
RSC - Rotor-side convert
VSC - Voltage source converter
PQ - Power quality
PQI - Power quality improvement
DG - Distributed generator
EPS - Electric power system
AEC - Alkaline electrolyser
PEMEC - Proton exchange membrane electrolyser
KOH - potassium hydroxide
APF - Active power filter
ESS - Energy storage system
BSS - Battery storage system
DoD - Depth of discharge
LFP - Lithium iron phosphate
NMC - Nickle manganese cobalt
CAPEX - Capital expenditure
OPEX - Operational expenditure

Chapter 1

Introduction

The world is moving towards more sustainable energy production creating pressure and opportunity for the development of renewable energy sources. One of the reasons for this development is the fact that the non-renewable energy sources that we rely on are starting to deplete. Burning of fossil fuels also contributes to climate change and affects human health. The United Nations General Assembly has set goals as part of "Agenda 2030" to not only increase sustainable energy production but also make energy available to a larger part of the human population [1]. In recent years the work towards a zero emission energy future in Europe has started in earnest. Coal-power plants are closing down and investment in green energy technologies is rising. The new energy system is likely to be built around renewable energy sources like wind and solar, hydrogen and bio-methane [2]. Hydrogen is a very good energy carrier and can be produced by splitting water molecules using electricity. The hydrogen can then be burned or used to produce electricity in a fuel cell with the only waste product being water. Hydrogen is thereby a completely renewable and emission-free fuel that can be used for automotive vehicles as well as grid energy storage. However, the technology around hydrogen needs to be developed further to reach its full potential. Bio-methane is produced from organic materials like food waste, it is not emission-free but it is carbon neutral as no new carbon is added to the global system.

The increasing demand of electricity is putting pressure on the existing infrastructure that is not designed to handle the increasing load. Therefore the electrical grid all around the world is being upgraded and integrated with the latest technologies to what is known as a Smart Grid. The goal of a Smart Grid is to optimize the energy flows between generation, distribution, storage and consumption, in order to maximize efficiency and profit. This is achieved through extensive monitoring of the power flows, and the possibility for interconnection and fast communication between the different actors, producers and consumers in the system. Smart Grids also make it easier to integrate renewable intermittent and distributed energy resources like solar and wind [3]. The change from a centralized to a distributed power generation system introduces some new challenges like maintaining power quality in the grid. The grid frequency depends on the load on the system which requires the grid to balance power generation to demand in real time. A good Smart Grid power generation system can provide services that improve stability, efficiency and reduce over-all energy consumption [4].

Having a controllable and observable energy production in an intelligent grid allows for independent micro-grids to be set up in places where lack of infrastructure does not allow for connection with the main grid or where localized energy is being generated [3]. A good example could be agricultural farms, with quite high power demands at certain times of the year and usually located in rather remote places far from the power grid. This Master Thesis can be seen in conjunction with a project at LTH that aims to *investigate technical solutions for the fully renewable operation of agricultural operations through electrification* which is coordinated by Volvo Construction Equipment AB [5].

To be able to meet fast consumer demand shifts it is important that part of the system is flexible and responsive. This makes solar power an excellent choice as part of a Smart Grid system as it can start producing energy very fast if the sun is shining. Of course one of the drawbacks of solar power in general is that power generation depends on weather which is unreliable. This project will focus on developing a unique concentrated solar power technology (CSP). The system is being developed by the company Stirlingversal and utilizes a Stirling engine, a reflecting dish and a gas burner to generate power. A Stirling engine is an engine that uses thermal energy to generate power making the technology principally different from the more known photovoltaic solar power technology. The goal of Stirlingversal is to further develop the system to make it marketable in the current marketplace. The company is developing the system to carry an additional power source that can boost the system when the incident solar power is low or nonexistent.

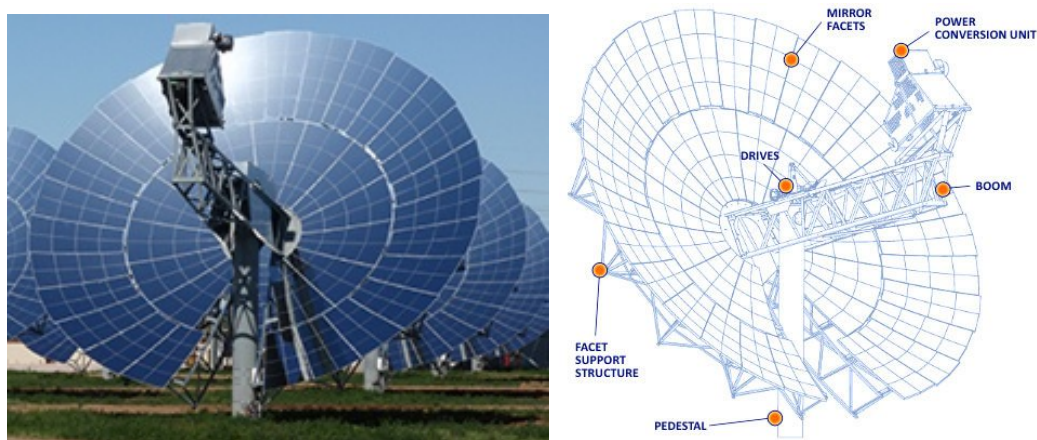


Figure 1.1: Image of the Stirlingversal Stirling-dish system and its functional parts

In this thesis a model of the Dish-Stirling system is developed including a model of the Stirling engine and the generator connected to the grid. A fixed speed generator configuration is modeled, compared with a variable speed generator configuration and power quality improvement methods are implemented in both systems. Lastly an electrolyser is modeled and integrated with the system. Hybrid mode operation is modeled and analyzed in terms of gas consumption for different irradiation conditions. The model results are then used to compare the hybrid Dish-Stirling system with a photovoltaic and battery based system of equivalent performance. The comparison is made at two potential locations that offer different solar power potential and are of interest from a market perspective: Lund (Sweden) and Johannesburg (South Africa). The viability of the system is analyzed in terms of cost and utility.

Chapter 2

Background

2.1 Stirling System History

The Stirling engine was invented by Robert Stirling in 1816 and the Dish-Stirling system was originally developed by McDonnell Douglas Corporation in the US who developed the dish and United Stirling AB of Sweden (now part of Kockums AB) who developed the Stirling engine in the 1980s [6]. In 1996 a company called Stirling Energy Systems (SES) was formed with the purpose of continuing the development of the solar dish system. In cooperation with DOE/Sandia National Laboratories they improved the dish to reflect 94% of incident radiation. They also developed the engine to be more cost effective. In 2005 they broke the previous power conversion efficiency record when they recorded 31.25% conversion efficiency on a cold day in May at Sandia's National Solar Thermal Test Facility. This is still the highest recorded conversion efficiency of any solar power plant. SES had signed a power conversion purchase agreement for 1,750 Megawatts which at the time would have been one of the biggest solar power plants in the world requiring around 70,000 mirrors. [7]. In 2008 NTR plc invested \$100 million in the company that was now developing what was described as two of the world's biggest solar power generation projects in the Imperial Valley and Mojave Desert [8]. SES declared bankruptcy in 2010 after the project developer Tessara Solar sold the initial project to a photo-voltaic company. Some cite the dropping price of photo-voltaic technology as cause for the failure while others blame bad management [9]. Today the energy market faces new challenges that have made the technology regain interest, Stirlingversal was formed to further develop the technology to meet the demands of the new market.

2.2 Dish-Stirling System

The Dish-Stirling system consists of a power conversion unit (PCU) and a parabolic mirror dish. Solar radiation is concentrated by the dish onto the receiver of the PCU. The receiver is thereby heated and that thermal energy is extracted by the Stirling engine. The Stirling engine in turn drives a generator that generate electrical energy. The receiver features a gas burner with an innovative combustion technology that maximises the burner efficiency and reduces NOX emissions to near zero. The burner can work with a wide array of fuels that includes: hydrogen, bio-methane and gas from industrial processes. What makes the Stirling system unique is that it uses the resultant heat from

the combustion instead of the resultant force from the gas expansion like in an internal gas combustion engine. This makes the engine able to burn the gas in a more controlled and effective way. In addition the combustion occurs outside of the engine, as a result the engine can use gas with lower quality than other systems. Gas from waste treatment plants, pyrolysis or metal forges could be used. Today these gasses are often considered to be waste products and burned emitting CO_2 into the atmosphere for no gain. Technically the engine could work with any heat source but the technology would have to be developed to be able to consume energy from for example solid fuels.

There are several benefits of the Dish-Stirling technology compared to other solar power solutions: the peak efficiency is as high as 30%, efficiency degradation due to time is very low and no rare unsustainable materials are used. Conventional solar panels typically have an efficiency of 18-22% [10]. More energy is consumed in the production of solar panels compared to the Dish-Stirling system [6], [11]. In addition the Dish-Stirling system produces waste heat in the form of warm water, if this energy is utilized the system efficiency becomes closer to 80-90%. The thermal energy could for example be used for heating of greenhouses or indoor environments, desalination plants or be used in some other process that requires thermal energy [6].

The main advantage of hybrid operation is flexibility. The energy generation is not strictly dependent on weather which could make it a good complement to intermittent power sources. When sun irradiation is lacking this system could still produce energy if needed as well as producing clean energy when the sun is shining. Furthermore, this additional energy can also be clean as long as the fuel comes from a sustainable source. The fact that it produces a secondary product in the form of warm water could make it a very cost-effective and reliable system for localized power generation where heat energy as well as electricity is needed. The system can run on hydrogen or bio methane which makes it possible to get the benefits of the hybrid operation with neutral CO_2 emissions and is in line with the general development and enthusiasm around moving toward a hydrogen and bio-methane based energy system.

No exotic or rare materials are used in the production of the system and according to Raghavaw [12] and less energy is being used compared to PV. The engine has some rotating inertia which helps stabilize the grid and the fact that the Dish-Stirling system uses an AC generator means that the system can be used without a power converter reducing cost and harmonic content.

The Stirlingversal dish system advantages:

- Has flexibility with hybrid operation
- Can play the role of both PV and fuel cell
- Produce waste-heat in form of warm water
- No exotic materials
- Supplies inertia to the grid
- Produces AC power (no power converters needed)

2.2.1 Engine Mechanics and Power Cycle

Ideally, the thermodynamic cycle consists of two isothermal and two constant-volume processes: isothermal compression, constant volume heat addition, isothermal expansion and constant volume heat rejection. The actual cycle, with crankshafts and sinusoidal motion of pistons only approaches the thermodynamic efficiency of the ideal cycle.

The engine consists of four cylinders, configured similar to figure (2.2) that are connected together in what is called the Siemens arrangement. The hot-side of every piston is connected to its neighbours cold-side. The larger the pressure difference between the hot and cold side the more powerful the stroke will be. The Stirling engine power cycle is shown in figure (2.1).

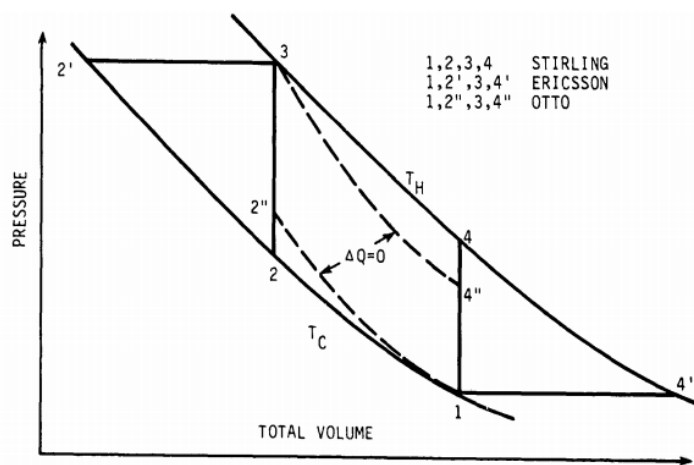


Figure 2.1: Theoretic Stirling, Ericsson and Otto cycle [13]

The gas is heated in the receiver tube which is connected to the hot side of the piston, the gas expands, pushing the piston down, this is how torque is generated. The gas is then forced back through the receiver tube where it absorbs more energy. Before the gas enters the cold side of the piston, the gas gives up a large part of its thermal energy to the regenerator. The gas then enters the cold side where it is cooled to maximize the pressure difference between the hot and cold side of the piston. When the piston is pushed down gas is forced back through the regenerator where the stored thermal energy is regained and used in the next stroke.

The temperature of the hot-side gas, which is inferred from the highest receiver tube temperatures, is held constant by controlling the amount of hydrogen gas circulating in the system. As the control tube temperature increases due to an increase in incident power, gas is added to the cycle from the storage bottle which increases the coolant flow through the receiver and brings the tube temperature back to the set-point value. When the tube temperature drops due to a reduction in incident power gas is removed from the cycle, compressed, and returned to the high-pressure storage bottle, which reduces coolant flow through the receiver and increases the working gas temperature [14].

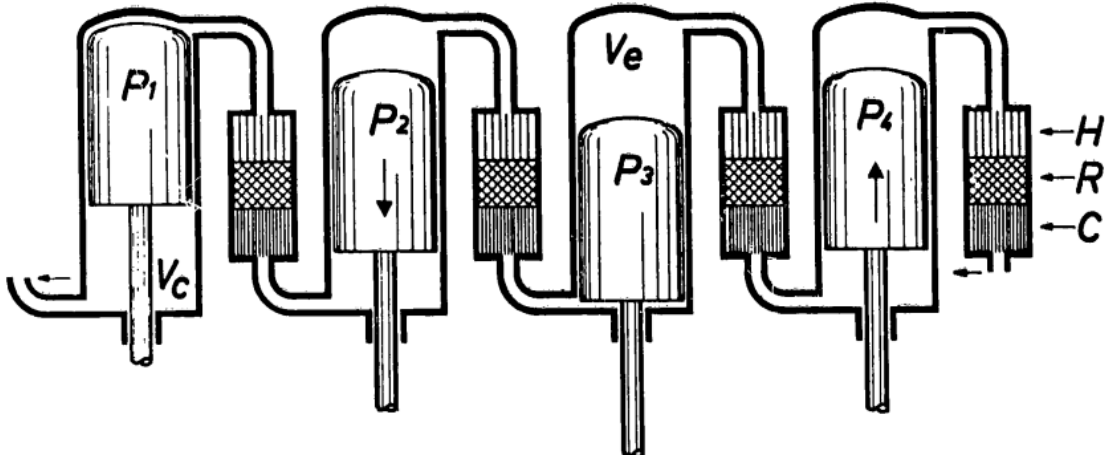


Figure 2.2: Stirling engine pistons arranged in the Siemens arrangement [13]

2.3 Photovoltaic systems

Photovoltaic (PV) solar technology has undergone an enormous development during the last 20 years. The most common PV technology today is Crystalline-silicon (c-Si) photovoltaic solar panels. Crystalline-silicon cells are made up several layers, glass, adhesive, anti-reflective coating and crystalized high purity silica. There are two major versions, single crystal c-Si which uses a single large crystal and multi-crystal c-Si which uses multiple crystal wafers. Commercial (c-Si) panels have a peak efficiency of around 18-22% and comprised 85% of world market sales in 2011 according to the US Department of Energy [10]. The production method is quite energy intensive, according to Raghava et.al [12].

Solar panels have recently become so competitively priced that they are often considered for new large scale power generation projects and are sure to play a big part in the future of green renewable energy. One of the greatest challenges with a PV system is that it only produces energy when the sun is shining, thus in order to be able to use all the energy that is produced during the day some energy storage device is needed. PV works with direct current (DC), however, the grid works with alternating current (AC). As a result the system requires DC-AC power converters to connect to the grid, this has to be taken into account, especially when PV generation comprises a large part of the energy mix.

2.4 Power Converters

Power converters are an integral part of the energy system, especially when it comes to many renewable energy sources. The grid uses AC but technologies like photovoltaics, fuel cells and batteries work with DC. Moreover, these technologies require conversion of DC power to AC power, which is done with power converters. Power converters can also be used to control AC power generators like in wind power plants or in the Dish-Stirling system as well as to provide services to make the grid more reliable.

Power converters basically work by switching the connection between two power lines

on and off in a certain pattern. For example if a converter intends to half the voltage from one power line to the other it will keep the lines connected 50% of the time by switching on and off rapidly and the resulting average voltage is reduced. Most power converters utilize this concept to varying degrees of complexity. To produce a sinusoidal waveform as would be the case with DC-AC converters the switching is done in such a way so that the most significant harmonic component of the resulting voltage waveform corresponds to the AC signal to be modeled. A filter is used to smooth out the waveform but converters like these still produce noise and harmonics on the line [15].

There are many different converter circuits and topologies but the main difference deciding the functionality of the converter rely on the switching components. Modern converters typically use IGBTs, they are power transistors that ore efficient and can be turned on and off. As a result an IGBT based converter has a high degree of control over the waveform it creates. The most commonly used three phase DC-AC and AC-DC converter device used in applications relevant to this paper is the Voltage Source Converter (VSC). The converter is usually based on IGBTs, it can transfer active and reactive power in both directions and work independently from the grid.

2.5 Power Quality

To ensure that electrical appliances and machines connected to the grid function correctly there needs to be some assurance of power quality (PQ). If the voltage drops or the frequency would change, electrical equipment might shut down or even be damaged. This can lead to huge problems in industry where startup-times can be several days for some processes. Therefore there are requirements on power providers to generate power with sufficient quality as to not affect the grid in a negative manner.

According to the European Standard EN 50160 and EN 61000 several quality aspects are regulated including:

- Rapid voltage changes are limited to 4%
- Power frequency ratio is limited to $\pm 1\%$
- Total harmonic distortion THD is limited to $< 8\%$
- Voltage magnitude variations $\pm 10\%$

Rapid voltage changes are changes in voltage that occurs in less than one second, this can be a result of a load being turned on. Power frequency ratio is the ratio of which the frequency deviates from the nominal frequency, the frequency for example decreases when there is less power being injected into the grid than is consumed. Therefore power production and consumption need to be actively balanced. Total harmonic distortion is a measure of high frequency power fluctuations on the grid. Non-linear loads can produce harmonics, power converters also produce them. Harmonic distortion can cause issues like resonance, overheating and tripping of protective equipment [16].

2.5.1 Active and Reactive Power

Electrical power is given by the product of voltage and current. In an AC-system, if the current and voltage phase is perfectly aligned the power will always be positive. However if the the current and voltage phase is not perfectly aligned there will be moments when the instantaneous power becomes negative and the total average power will decrease. If the current has a phase-shift of 90° the resulting average power would be 0 and no useful work would be performed. This led engineers to introduce the concept of complex power: the power is divided in to a real part that contributes to useful work and an imaginary part that does not. Basically you could say that the currents sinusoidal waveform is expressed as the sum of two sinusoidal waveforms, one in phase with the voltage and the other 90° out of phase. The in-phase part that contributes to useful work is called active power and the out-of-phase part that does not contribute to useful work is called reactive power. The power-factor of a system is given by $\cos(\phi)$ where ϕ is the phase shift angle and describes the relation of reactive power to active power in the system. Reactive power is produced by inductors and capacitors, certain loads or power generators will introduce it into the system.

2.5.2 Power Quality Improvement Methods

In order to mitigate disturbances and other PQ problems power quality improvement (PQI) methods have been developed. These consist of electrical hardware and software components that work to rectify PQ problems that arise. There are many different methods that can be applied, generally providing the following functions:

- Voltage regulation
- Active power regulation
- Reactive power regulation
- Harmonic compensation
- Load feeding

In general PQI methods use a combination of power converters and filters to achieve the desired result. This work will apply two methods in particular: the active power filter (APF) and the multi-functional power generator.

Active Power Filter

The active power filter consists of a power inverter and an energy storage, usually in the form of a capacitor. The capacitor is charged so that a certain voltage is achieved. The power inverter is used to compensate for voltage sags, harmonics and reactive power by injecting or absorbing currents to and from the grid [16].

Multi-functional power generators

A lot of power generation systems use some form of power converter in order to inject active power to the grid. The hardware and configuration is often very similar to an active power filter. The multi-functional power generator is simply a system that uses the hardware that it already requires in order to provide ancillary services like harmonic compensation or reactive power regulation.

2.6 Generators

Generators are used to produce electric power from mechanical power. The most widely used are rotary generators, consisting of a stator and a rotor, the stator is stationary while the rotor rotates. Mechanical force is converted to electricity when the magnetic fields which are induced by a phenomena called induction and described by Faraday's law, emanating from the rotor and stator interacts with each other. In a generator the external force causes the induced magnetic field to vary in a way that generates current. Depending on the mechanical rotational speed of the rotor in relation to the frequency of the electric power generated, generators can be divided into two different groups: asynchronous machine (AM) and synchronous machine (SM). The distinction is that in synchronous generators the rotor rotates with the same frequency as the magnetic field emanating from the stator. In the asynchronous machine the rotor frequency and the magnetic frequency differ under load which makes it harder to control [15]. Examples of synchronous machines are the Electrically Magnetized Synchronous Generator (EMSG) and the permanent magnet synchronous generator (PMSG). Both are used in power generation applications when variable speed operation is required. These generators can operate from zero rotational speeds but are relatively expensive. They also need full power converters in order to connect to the grid [17]. An example of an asynchronous machine is the induction generator, which is one of the generator that is used in this work.

2.6.1 Induction Generator (IG)

The induction generator is an asynchronous machine and is the most commonly used generator due to its simplicity and low cost. In addition the generator can be constructed without brushes and slip-rings which results in higher reliability and lower maintenance costs. The class of generators gets its name because it lacks a dedicated source of magnetic flux in the rotor, so it relies on inducing rotating magnetic fields (rmf) that produce torque. There are two types of induction generators that are relevant to this work.

Squirrel Cage Induction Generator (SCIG)

The SCIG has a short-circuit rotor constructed of aluminum or copper bars that are short-circuited by two conductor rings. The construction resembles a cage which is where the machine gets its name. The design of the rotor determines startup characteristics and at what speed the generator operates at optimal efficiency. Even though power electronics can be used to control speed and torque the existence of rotor currents (as compared to the PMSG) leads to a somewhat lower efficiency than a PMSG. .

Doubly Fed Induction Generator (DFIG)

The DFIG is very similar to the SCIG, the difference is that the rotor features windings that can be connected to a power converter via slip rings. This makes it possible to alter the electrical characteristics of the rotor during operation. In this way, the torque speed and reactive power of the generator can be controlled. This can be done with converters with a fraction of the power rating compared to synchronous generators. Compared to the SCIG, the downside is added cost and required maintenance.

2.7 Conversion Topologies

Due to lack of information and research on sterling energy conversion systems a survey has been made on similar systems in wind energy conversion. Wind energy conversion systems (WECS) use generators and are driven by a force that is variable, thus they face the same kind of challenges as a Dish-Stirling system. There are a couple of different wind energy conversion systems in use today with different benefits and drawbacks. One of the main differences between WECS and Dish-Stirling systems is that the Stirling engine works at much higher frequencies, some topologies for WECS need gearboxes to match the rotor speed of the blades to the generators optimal speed. This would not be necessary with a Dish-Stirling system where the engine operates at similar speeds as a grid connected induction generator.

2.7.1 SCIG Conversion Systems

The simplest conversion system is a SCIG fixed speed conversion system directly connected to the grid. Here the generator will always operate at the 50Hz, and some PQI device will be needed if reactive power compensation is required. This system is very robust and does not require brushes or slip rings. Since it operates at a fixed speed, power fluctuations are directly translated to torque, which can be damaging. The generator is self excited, which means that it needs the grid to operate and has no ability to support the grid through disturbances. A soft-starter can be used to mitigate the otherwise high starting current of the generator.

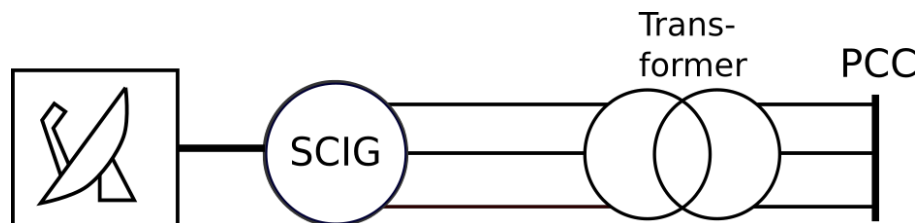


Figure 2.3: SCIG system topology

[18].

2.7.2 DFIG Conversion System

One of the most common wind energy conversion systems are based on the DFIG. The torque and speed is controlled by controlling the currents on the rotor windings. The system can be designed to make the generator able to deviate by $\pm 30\%$ from the grid frequency. In that case the rotor supply (illustrated by the power converters in fig 2.4) only needs to supply 30% of the rated power. The rotor supply generates the full torque in the rotor but at $\pm 30\%$ of the synchronous speed which makes the power flow decrease by the same amount. The reactive power consumption of the generator can also be mitigated by the rotor supply. The generator is robust and has a relatively low price. The main downsides are that the generator uses slip-rings which causes the system to need more maintenance, the system is also susceptible to grid disturbances and has difficulty complying with grid low voltage ride through requirements [19].

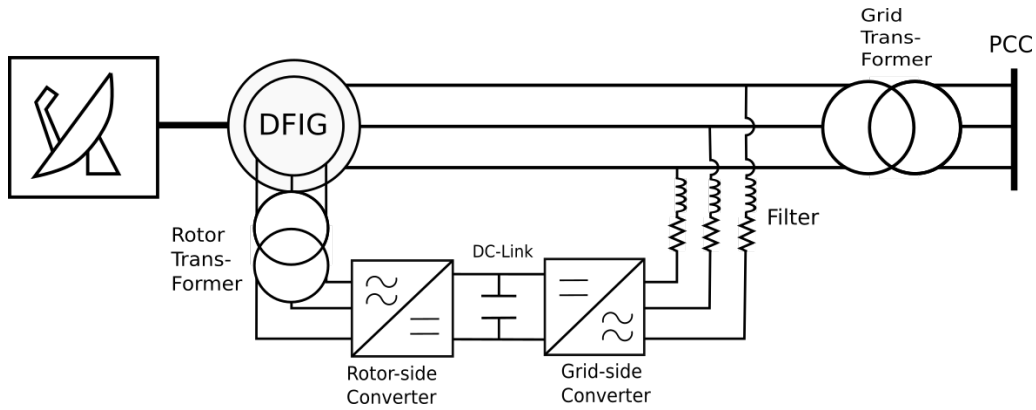


Figure 2.4: DFIG system topology

2.8 Energy Storage

One of the biggest challenges with renewable energy is the fact that we don't have control over the source in some cases. In the example of solar we might have abundant energy during the day but none at night. This is of course not acceptable in the society we live in and if renewable intermittent energy sources are to be widely accepted it is a problem that needs a solution. Energy needs to be stored from times when it is abundant to be available when it is not, this is done with an energy storage system (ESS). There are some challenges when storing energy at utility power-scale. The amount of energy that needs to be stored is very large and the ESS needs to be able to output enough energy to satisfy demand. The response-time of the system determines how fast changes in energy demand can be rectified. The amount of time the energy can be stored limits how well the system handles longer weather variations.

Several technologies are used for energy storage and are suited for different applications. For very large scale applications technologies like pumped hydro and compressed air storage are used and for middling and small scale systems (1-100MW) the most common storage technology is the battery. The Dish-Stirling system in this work operates at lower power levels so focus is given to the battery technologies, the fact that the system uses thermal energy makes the possibility of thermal storage an option as well.

2.8.1 Batteries

Battery storage systems (BSS) can be used for energy storage at utility scale, and systems with up to 100MW power output and 250MWh of storage capacity have been installed [20]. Two of the most attractive properties of battery technologies are the round trip efficiency and the response time. High round trip efficiency means that a low amount of energy is lost in the process. The low response time allows the system to respond quickly to grid fluctuations, balancing the grid and making it more reliable. There are some shortcomings with battery systems as well: Energy cannot be stored for a long time, the price of a BSS is higher than other large-scale options and the materials used are not the most environmentally friendly. The equivalent GHG emissions associated with the production of 1kWh of energy storage is 61,000gCO₂ for lithium-ion batteries [21]. Another thing to consider with a BSS is that a battery operates with direct current which means that grid integration will require some power-electronics.

Lithium-ion Battery

Lithium-ion batteries are used in applications from mobile phones to electric vehicles. Compared to other battery technologies it enjoys very high energy density. There are two main Lithium-ion technologies that are used for energy storage: iron-phosphate (LFP) and nickel manganese cobalt (NMC). NMC has high energy density and is therefore lighter, it is often used in electric vehicles. LFP batteries have a longer lifetime and it is more suited for energy storage if size and weight is not a critical factor. The system has a high round trip efficiency of 86 - 88%, and a very fast response time of 1-4 seconds. The lifetime varies depending on use but more than 10 years is difficult to achieve [22], [23]. The cost of a Lithium-ion battery based systems is decreasing due to the development in the electric vehicle industry but is still quite high.

2.8.2 Thermal Storage

Thermal energy storage takes thermal energy and stores that energy for later use. This can be done in a few different ways like utilizing chemical reactions for example. The most applicable method for a Dish-Stirling system would be what is called latent thermal energy storage. An energy carrying material is heated up when demand is low and extracted when demand raises, the material is encased in a thermal insulator which allows the energy to be stored for longer amounts of time than that of a battery. The material can be organic, like water or rock, but in the case of high temperature storage inorganic materials like metal alloys or salts are used. In the case of inorganic materials the phase change properties of the materials are exploited, as a salt or metal melts or solidifies it keeps a constant temperature but energy is stored in the phase transition. The phase transition temperature of the material can be chosen to be the same as the working temperature of the system.

According to Khare et.al [24] the equivalent GHG emissions associated with producing 1000kWh of energy storage using an aluminum-silica alloy is 6,443kg. In comparison the GHG emission associated with 1000kWh hours of lithium-ion storage would be 61,000kg [25]. Thermal storage has a very attractive carbon footprint in comparison to battery technologies and metals do not degrade over cycles making long life times possible. The effectiveness of charging and discharging can be as high as 80-90% with aluminum. There are some challenges with this kind of energy storage as well, mostly having to do with the weight of the system, thermal conductivity, corrosion of containers and heat exchange piping [24]. There are few thermal storage system of this type in the world but the technology carries a lot of potential .

2.9 Electrolysis

Electrolysis is the reversible process commonly referred to as splitting water. The process uses electricity to divide the H_2O molecule into hydrogen and oxygen. The devices that implement this process are called electrolyzers, devices that reverses the process, producing electricity and water from hydrogen and oxygen are called fuel cells. The electrolyser consists of four major parts: anode, cathode, membrane and electrolyte. The process occurs on the cathode and anode with the help of catalytic materials, the membrane sep-

arates the anode where oxygen is released from the cathode where hydrogen is released. An example of an alkaline electrolyser is shown in fig (2.5)

Electrolysers have long been used in industry to produce high purity hydrogen for different industrial applications. In recent years the interest for hydrogen as energy storage for renewable energy production like solar and wind has increased. This new use-case add new requirements to the electrolysers and is something that is being studied. One of the main issues with hydrogen production with intermittent energy sources is that the electrolysers operate optimally in static conditions. Power fluctuations can lead to decreased efficiency, cell corrosion and increase in gas crossover between the anode and cathode. The latter is especially worrying since the mixture of hydrogen and oxygen can become explosive. To overcome these issues the technologies are being developed in different ways. The most common electrolyser technologies today are alkaline electrolysers (AEC) and proton exchange membrane electrolysers (PEMEC). PEMEC electrolysers are a relatively new development that aims to reduce the size of the electrolyser as well as improve the dynamic properties making them more suitable for intermittent energy sources. Due to the reliability of the hybrid Dish-Stirling systems energy generation the AEC is the technology that is considered, due to the higher technology maturity and lower price.

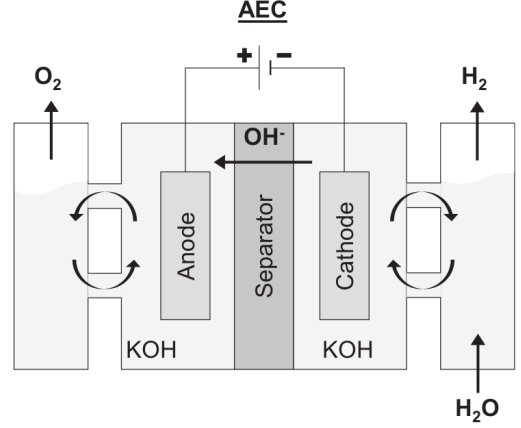
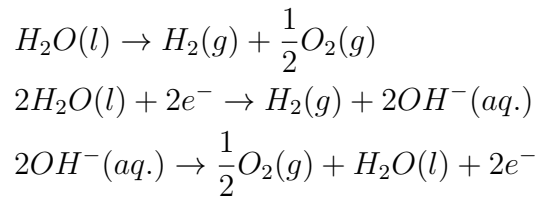


Figure 2.5: Alkaline electrolyser [26]

2.9.1 Alkaline Electrolysis

Alkaline electrolysis is a mature and sustainable technology that has been used since the 1920s and has relatively low capital cost. The main disadvantages with AEC is that the current density is quite low which results in larger devices and the dynamic performance is also worse than the PEMEC. A potassium hydroxide (KOH) solution is typically used as the electrolyte. Nickel or nickel-molybdenum (Ni, Ni-Mo) alloy is typically used for the cathode and nickel or nickel-copper alloy (Ni, Ni-Cu) is used for the anode [26].

The fundamental equations of alkaline water electrolysis:



One of the main problems with an alkaline water electrolyser combined with intermittent energy sources like solar or wind is the partial loading issue [27], alkaline electrolysers function best in static conditions and have comparatively poor dynamic properties. One

focus of the development of AECs is the dynamic performance [26], others have proposed an addition of a battery system to solve the issue [27].

2.10 Distributed Generation & Local Networks

In order to create an emission free and sustainable world fossil fuels need to be replaced with clean alternative energy sources. This means that the infrastructure that allows electrical energy to be distributed will need to be expanded to accommodate the load. Traditionally the power grid functioned with large centralized energy production that was distributed in bulk by the grid. In order to reduce losses on the transmission lines the voltage is transformed via substations to levels over 100kV. The voltage then has to be transformed back to a usable level where the consumer is located. This is not a perfect system as there are still losses in the transmission, bottlenecks can occur between power generating areas and consumers and it is very costly to expand [28].

This is the reason why distributed generation (DG) is considered an interesting option for electrification. Many renewable resources are not confined to one particular area which can make it possible to produce the power in the same area as where it is consumed. This reduces the load on the main grid and at the same time makes it more robust. Energy lost in transmission is reduced and less money has to be spent expanding the capabilities of the grid. In some remote areas the grid is too weak to be reliably used, take for example a farm where it would be too expensive to build a reliable grid connection but a lot of energy is needed to run equipment and environment control. There, a DG system could be much more cost efficient and allow the operation to be electrified.

DGs have their own challenges and things to consider. When the DG is providing a large fraction of the energy consumed by an electrical power system (EPS), the PQ and controllability of the generated power becomes more important. For example injecting or consuming reactive power can lead to under or over-voltages down the line. More consideration has to be taken to what loads the EPS supplies and what kind of power-factor they need. If there is a fault on the EPS the DG needs to be able to respond in an appropriate time as to not damage electrical equipment or itself [28].

Chapter 3

Dish-Stirling Model

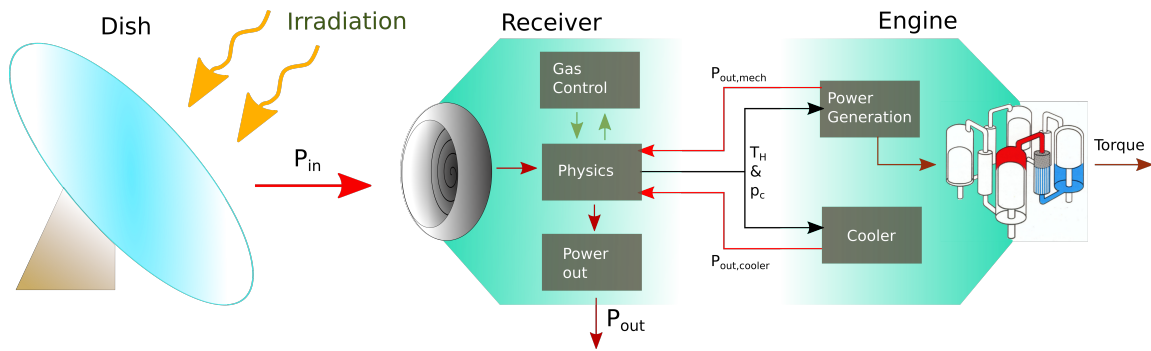


Figure 3.1: Overview of Dish-Stirling model

The models used in this thesis are built in MATLAB Simulink. The Stirling engine model was developed in this work, the generator models are ready made models in MATLAB. The Stirling PCU model is built up of two main parts: receiver, and engine. The receiver takes the incoming power, outgoing power and working gas mass to compute the hot side temperature and pressure. The engine block takes the temperature and pressure to calculate torque that is applied to the generator and the resulting outgoing power as well as outgoing thermal energy.

3.1 Receiver

The receiver of the Stirling engine consists of metal pipes that get heated by concentrated solar radiation or a flame. The receiver is modeled as a single mass where heat transfers homogeneously.

3.1.1 Incoming Power & Losses

Energy-loss due to reflection irradiation, convection and similar are simulated as a percentage loss derived from operational data at peak energy production. In hybrid operation the incoming energy consists partly of concentrated solar radiation and partly of heat generated by gas-combustion. The gas burner uses a very efficient combustion technology as well as heat regeneration from the exhaust of the burner. No data is currently available on how efficient this system is and the efficiency is therefore assumed to be 85%. This figure is derived by assuming similar efficiency as is obtained with concentrated radiation

with the omission of the energy loss caused by reflectivity in the mirror.

The energy losses in the receiver are obtained from Lopez [14]:

Source	Value
Reflectivity	91%
Intercept	96.7%
Receiver	90%
Temperature diff	99.5%

Table 3.1: System energy loss

Reflectivity losses are losses due to imperfections in the mirror. Intercept refers to losses due to tracking error and mirror cant errors due to wind and similar. The receiver losses account for energy radiating back out of the receiver and other heat losses. The temperature difference loss is losses due to temperature difference across different receiver tubes.

The radiation energy reaching the PCU is calculated by applying these losses to the total energy captured by the dish.

$$P_{in} = P_{DNI}A_{dish}\gamma_{loss} \quad (3.1)$$

P_{DNI} = Incoming direct normal irradiation (W/m^2)

A_{dish} = Projected area of dish (m^2)

γ_{loss} = Cumulative losses

3.1.2 Physics

The physics block calculates the hot-side temperature of the receiver, that is the temperature of the receiver tubes and the gas flowing through them. It also calculates the engine pressure as a result of gas flowing in and out of the system.

Temperature

The energy coming in to the PCU is what drives the temperature to increase. The PCU converts that energy to work and thermal energy that is carried out by the coolant. The temperature change of the receiver is derived by the balance of the incoming and outgoing power:

$$\frac{dT_m}{dt} = \frac{P_{in} - P_{out}}{m_m C_{pm}} \quad (3.2)$$

P_{in} = Power in (W)

P_{out} = Power out (W)

m_m = Receiver metal mass (kg)

C_{pm} = Specific heat constant ($JK^{-1}kg^{-1}$)

The outgoing power is calculated in the engine block. Hot-side temperature is then calculated by integrating the temperature change expressed in the equation. The dynamics of the heat transfer are not simulated as this is not the focus of the study. Instead this model is meant to simulate the average temperature over many cycles.

Pressure

The hot-side temperature is controlled by increasing or decreasing the pressure of the working gas. If the receiver is getting too hot increasing pressure results in a decrease of temperature, a higher pressure allows the engine to transfer more of the incoming energy into work and warm water. The gas control algorithm is a company trade secret and will not be discussed in this report. The physical system consists of one high pressure container and one low pressure container, when the pressure needs to be changed on the cool side of the engine is connected to the appropriate container via a solenoid valve and gas flows in or out of the system.

p_c = Engine pressure, cold side (*bar*)

p_s = Source pressure, container (*bar*)

D = Pipe diameter (*m*)

A_{pipe} = Pipe area (m^2)

L = Pipe length (*m*)

v_g = Gas flow velocity (*m/s*)

ρ = Gas density (kg/m^3)

ν = Kinematic viscosity (m^2/s)

When the control system sends a signal either the low pressure or high pressure valve is opened transferring gas out or in to the PCU. The gas flow velocity due to pressure difference between the gas container and PCU is calculated using the Bernulli equation:

$$p_1 + \frac{1}{2}v_1^2 + \rho gh_1 = p_2 + \frac{1}{2}v_2^2 + \rho gh_2 + f_h \rho g \quad (3.3)$$

The friction head loss is given by the Darcy equation:

$$f_h = f \frac{Lv^2}{2Dg} \quad (3.4)$$

Assuming no head loss due to gravity gives gas flow velocity:

$$v_g = \sqrt{\frac{4D(p_s - p_c)}{2D - fL\rho}} \quad (3.5)$$

$$Re = v_g D / \nu \quad (3.6)$$

The gas pipe is assumed to be straight with no bends and the flow is assumed to be laminar which gives friction factor:

$$f = 64/Re \quad (3.7)$$

Following this the massflow becomes:

$$\dot{m} = \rho v_g A_{pipe} \quad (3.8)$$

The pressure is then calculated by the ideal gas law:

$$p = \frac{\int \dot{m} dt}{V_e} TR_e \quad (3.9)$$

3.2 Engine

The engine block is responsible for calculating the resultant mechanical power and torque produced by the engine. It also calculates the power flowing out of the engine as a result of heat energy transferring from the gas to the coolant and other losses.

3.2.1 Mechanical Power Generation

A fully detailed model of the engine is not within the scope of this project and therefore a simplified model is developed. The model is based on the calculations presented in [13] where Martini states that the ideal work produced from one Stirling cycle can be expressed as:

$$W = W_C + W_E \quad (3.10)$$

$$W_C = nRT_C \ln \left(\frac{V(2)}{V(1)} \right) \quad (3.11)$$

$$W_E = nRT_H \ln \left(\frac{V(1)}{V(2)} \right) \quad (3.12)$$

W_C is the compression work and W_E is the expansion work. The volumes $V(1)$ and $V(2)$ are constant and depend on the engine design, n is the number of moles hydrogen. T_H and T_C is the hot-side and cold-side temperatures respectively. It is also noted that the compression work is negative and that $\ln(V(2)/V(1)) = -\ln(V(1)/V(2))$. The work resulting from one Stirling cycle can thus be expressed as:

$$W = nR \ln \left(\frac{V(1)}{V(2)} \right) (T_H - T_C) \quad (3.13)$$

Multiplying with the number of cycles per second (f (Hz) = $\frac{\omega}{2\pi}$ (rad/s)) gives the power. Comparing this to the equation for work dependent on torque (τ_{mech}) and rotational speed (ω) gives an expression for the produced torque from the four pistons of the Stirling engine:

$$P_{out} = \omega \tau_{mech} = 4 \cdot \frac{\omega}{2\pi} nR \ln \left(\frac{V(1)}{V(2)} \right) (T_H - T_C) \quad (3.14)$$

$$\tau_{mech} = \frac{2}{\pi} C_\tau nR (T_H - T_C) \quad (3.15)$$

Where $C_\tau = \ln \left(\frac{V(1)}{V(2)} \right)$. In order to approximate C_τ data from [6] (Table III-2) is used, this is data from a precursor of the Stirlingversal system and the performance is assumed to be similar. The engine has an efficiency of 42% (γ_e) at $1000W/m^2$ (P_{in}) irradiation,

mirror area $87.6m^2$ (A_D) at a rotational speed around 188.5 rad/s (ω) and a temperature difference of $(720-50 = 670)$. The power equation is given by:

$$P_{out} = \omega \frac{2}{\pi} C_\tau n R (T_H - T_C) \quad (3.16)$$

$$C_\tau = \frac{\pi P_{out}}{2\omega n R (T_H - T_C)} \quad (3.17)$$

The engine has a maximum cold side pressure of 200bar and a displacement volume of 95cc per piston. If no dead space is assumed and the volume of regenerator and receiver tubes are neglected the number of moles can be calculated by the ideal gas law:

$$p_{200} V_{95} = n_{max} R T_C \rightarrow n_{max} = \frac{p_{200} V_{95}}{R T_C} \quad (3.18)$$

P_{out} is equal to $P_{in} \gamma_e$ which gives:

$$C_\tau = \frac{\pi T_C P_{in} \gamma_e}{2(T_H - T_C) \omega p_{200} V_{95}} = 0.14 \quad (3.19)$$

It should be noted that the real engines' cycle is not ideal, the C_τ constant contains an assumed linear correlation between the ideal cycle and the actual engine. This is a simplification. In order to make the model more realistic the efficiency variation due to engine pressure is taken into account; Martini [13] shows that the Stirling efficiency is a function of rotational speed and engine pressure, the data from Lopez [14] is derived from a system with close to constant rotational speed, therefore the system efficiency is assumed to be a function of the engine pressure. The system is simulated with a constant engine efficiency of 42% and engine pressures at different irradiation levels are noted. A polynomial is then fitted to the efficiency values derived from Lopez and the pressure values derived from the simulation. For a more accurate result this process could be iterated with the polynomial replacing the constant efficiency but this was deemed unnecessary. The difference in pressure between the hot and cold side of the engine was used for the efficiency calculation. The resulting efficiency polynomial and values can be seen in table 3.2 and figure 3.2.

W/m^2	200	300	400	500	600	700	800	900	1000
$\Delta P(bar)$	91	137	180	224	268	311	353	394	415
$\gamma_e(\%)$	14.23	24.85	30.15	33.34	35.46	36.98	40.03	40.70	42.47

Table 3.2: Pressure difference values and engine efficiency at different irradiation values

The engine engine torque is thus a function depending on the engine pressure, the correlation is defined as $K_\tau(\Delta p)$:

$$K_\tau(\Delta p) = \frac{\pi T_C P_{in} A_D \gamma_e(\Delta p)}{2(T_H - T_C) \omega p_{200} V_{95}} \quad (3.20)$$

The torque generated by the engine is calculated as:

$$\tau_{mech} = \frac{2}{\pi} K_\tau(\Delta p) n R (T_H - T_C) \quad (3.21)$$

Thus the equation for generated mechanical power is defined as:

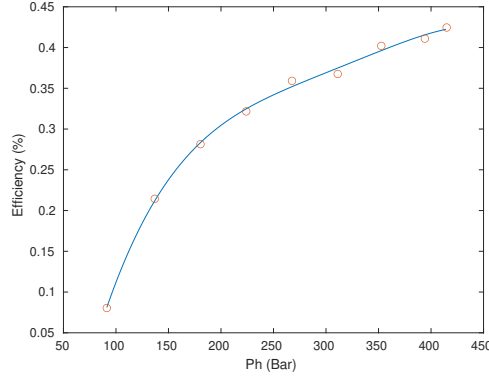


Figure 3.2: Efficiency correlated to pressure, the line represents the $\gamma_e(\Delta p)$ polynomial

$$P_{out,mech} = \omega\tau_{mech} = \frac{2\omega}{\pi}K_\tau(\Delta p)nR(T_H - T_C) \quad (3.22)$$

3.2.2 Cooler

The cooler is responsible for maximizing the temperature difference between the hot side and cool side resulting in more torque. The modeling of the cooler is very simplified. The efficiency of the engine is a measure of how much energy it converts into work, the remaining energy is consumed by the cooler and other losses. The energy transferred by the cooler and other losses is thus calculated as:

$$P_{out,cooler} = \frac{1 - \gamma_e(\Delta p)}{\gamma_e(\Delta p)}P_{out,mech} \quad (3.23)$$

It is simply the exact same calculation as for $P_{out,mech}$ but with an efficiency of $(1 - \gamma_e(\Delta p))$

Chapter 4

Electrical Models

4.1 Induction Generator Mathematical Model

The generator models are defined around the governing electrical equations of the asynchronous generator (fig 4.1). Both the DFIG and SCIG can be modeled by these equations. The difference is that in the case of the SCIG the rotor is short-circuited which makes $\bar{u}_r = 0$ and in the case of the DFIG \bar{u}_r can be controlled in order to produce a desired result.

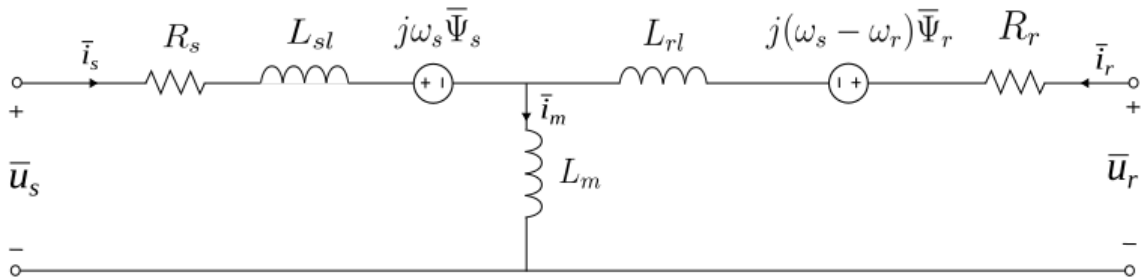


Figure 4.1: Equivalent circuit representation of the induction machine

R_s Stator resistance

L_{sl} Stator leakage inductance

$\bar{\Psi}_s$ Stator flux vector

ω_s Stator frequency

L_m Magnetizing inductance

R_r Rotor resistance

L_{rl} Rotor leakage inductance

$\bar{\Psi}_r$ Rotor flux vector

ω_r Rotor frequency

$$L_s = L_m + L_{sl} \quad (4.1)$$

$$L_r = L_m + L_{rl} \quad (4.2)$$

The equations governing an induction machine are:

$$\bar{u}_s = R_s \bar{i}_s + \frac{d\bar{i}_s}{dt} L_{sl} + j\omega_s \bar{\Psi}_s + \frac{d\bar{i}_m}{dt} L_m \quad (4.3)$$

$$\bar{u}_r = R_r \bar{i}_r + \frac{d\bar{i}_r}{dt} L_{rl} + j(\omega_s - \omega_r) \bar{\Psi}_r + \frac{d\bar{i}_m}{dt} L_m \quad (4.4)$$

$$\bar{\Psi}_s = L_s \bar{i}_s + L_m \bar{i}_r \quad (4.5)$$

$$\bar{\Psi}_r = L_m \bar{i}_s + L_r \bar{i}_r \quad (4.6)$$

The generator parameters were chosen as:

Variable	Value	Variable	Value
Rated Power	30kW	Rotor Resist (R_r)	0.3Ω
Frequency (f_s)	50Hz	Stator Induct (L_s)	102.4mH
Stator/Rotor Volt	400/300V	Stator Resist (R_s)	0.24Ω
Magnet Inductance	100mH	Inertia (J)	0.467K gm ²
Rotor Induct	102.4mH	Friction (B)	0.01K gm ²

Table 4.1: Generator parameters

The generator has two pole pairs and the parameters were chosen as very similar to those presented in Mendes et.al [29]. It should be noted that these parameters are not optimized for this application and performance might be enhanced with differing generator parameters.

4.1.1 Torque generation

In the asynchronous machine a rotating magnetic field (rmf) is generated by the stator windings as three phase alternating current is run through the windings. Most of this magnetic field passes over the air gap between the stator and rotor where it intersects the rotor. The rotor is built up of conductors that are perpendicular to the stator rmf. In accordance with Faraday's law alternating current is induced in the rotor. This in turn gives rise to a rmf generated in the rotor. The torque in an asynchronous machine is produced as the magnetic fields generated from the stator interacts with the currents generated in the rotor and visa versa. This can be expressed as the result of the Lorentz force law, the current carrying conductor that is the rotor is immersed in the magnetic field generated by the stator, thus the rotor experience a force perpendicular to the current. This is the torque. Mathematically the torque can be expressed in several different ways as shown in [15]:

$$T_{el} = \bar{\Psi}_s \times \bar{i}_s = \bar{\Psi}_r \times \bar{i}_r = -\frac{L_m}{L_r} \bar{\Psi}_s \times \bar{i}_r = \frac{L_m}{L_r} \bar{\Psi}_r \times \bar{i}_s \quad (4.7)$$

It should be noted that the maximum torque is acquired when the flux and current vectors are perpendicular to each other.

The the rotational speed of the generator is determined by the electromagnetic torque as well as the mechanical load torque according to:

$$\frac{d}{dt}(J\omega) = T_{el} - T_{mech} \quad (4.8)$$

In the SCIG the rotor consists of bars in the resemblance of a cage. An important thing to understand about the the torque generation in the SCIG is that for current to be induced in the rotor the rmf of the stator has to be in motion in relation to the rotor conductors. This means that the rotor can never rotate at the same speed (synchronous) as the stator rmf as this would result in the relative rotational speed between stator rmf and rotor being zero. The rotational speed difference between the stator rmf and the physical rotor is called the slip and is defined as $\omega_{slip} = \omega_s - \omega_r$. The alternating current induced in the rotor will therefore have the frequency of the slip, generating a rmf that rotates at the slip frequency in relation to the rotor. The fact that the rotor at this point has the rotational frequency of $\omega_r = \omega_s - \omega_{slip}$ means that the combined rotational frequency of the rotor rmf in relation to the stator is: ω_s . What this means is that the rotor rmf and the stator rmf rotates at the same frequency even if the rotor does not. If this was not the case the generated torque would never be constant. When the SCIG is connected directly to the grid as in figure 2.3 the torque is controlled by the grid frequency. If the mechanical torque should increase the speed of the rotor will increase slightly, then according to Faraday's law the magnitude of the rotor current increases which in turn increases the electromagnetic torque until an equilibrium is found. The higher the torque an SCIG is subjected to the larger the slip frequency will become.

4.1.2 Reactive Power Control

A normal induction generator consumes reactive power as an inherent result of the inductance of the rotor and stator windings. As alternating voltage is applied to the phases the current will lag behind according to ohm's law: $V = L \frac{dI}{dt} + RI$. It can be noted that this phase lag will decrease the larger the resistance of the winding is but higher resistance also results in higher losses.

With the DFIG configuration the rotor flux $\bar{\Psi}_r$ can be controlled to some degree. Just like when the stator flux wave induces currents in the rotor the rotor flux has the same effect on the stator windings. Therefore it is possible to adjust the rotor flux wave's angular position in relation to the stator current so that the induced stator currents cancel out the currents responsible for the reactive power. In this way reactive power can be controlled.

4.1.3 Speed Control

The factor that limits the rotor speed of the SCIG at super-synchronous speeds is the slip. As the slip increases more current is induced in the rotor and at some point the heat generated by the resistance of the windings can not be dissipated fast enough and the winding will burn out. At sub-synchronous speeds the current that is generated will be inverted, creating torque in the opposite direction working as a motor. This is the reason why induction generators always work at super-synchronous speed and induction motors always work at sub-synchronous speeds.

In the DFIG configuration however the rotor currents are controlled. The operation of a SCIG is defined by the slip or to be more accurate it is defined by the relation of the rotor current phase to stator current phase. If the rotor current lags behind the machine operates as a motor, if the rotor current is leading the machine operates as a generator. If the DFIG is operated at super-synchronous speeds the current phase is controlled to produce the desired amount of torque and is at the same time limited as to not overheat the windings. This results in less current flowing through the windings making it possible for the rotor to spin faster. In this case power will be flowing from the rotor to the grid via the rotor supply. At sub-synchronous speeds however the converters need to control the rotor current phase so that it leads in relation to the stator current. Power will in this case flow from the grid to the rotor.

4.2 DFIG Control system

The DFIG system has two power converters, one connected to the rotor terminals and one connected to the grid, they are in turn connected via the DC-link. These are called the rotor-side converter and the grid-side converter and they each execute their own control algorithms. The rotor side controller is able to control the torque and thereby the rotational speed of the generator as well as compensate for reactive power consumed by the generator. The grid side converter controls the DC-link voltage and compensates for reactive power originating from other sources. The DFIG model is based on a model built by Richard Gagnon [30], the algorithm and model is considerably altered with original work and methodology derived from Snyder [31] and Fletcher [32].

4.2.1 Rotor-side Converter Control

The rotor-side converter (RSC) control system is depicted in figure 4.2 and the different parts of the algorithm will be explained in the following sections.

Torque Current Control

Torque is difficult to measure, therefore the current reference value relating to torque production is controlled in an open loop manner. In this system the torque controller is cascaded with the speed control loop so that the torque is indirectly controlled by the speed controller. As mentioned before and as shown in the equation 4.7 the torque of the generator can be described by a relationship between rotor current, stator flux:

$$T_{el} = -p \frac{L_m}{L_r} \bar{\Psi}_s \times \bar{i}_r \rightarrow T_{el} = -p \frac{L_m}{L_r} (\Psi_{sd} i_{rq} - \Psi_{sq} i_{rd}) \quad (4.9)$$

The number of generator pole pairs is represented by the variable p . The Park transform is chosen so that the q-axis is aligned with \bar{u}_s , steady state conditions are assumed. Equation 4.3 then gives that $\Psi_{sq} = \frac{R_s i_{sd} - u_{sd}}{\omega_s}$. Due to the axis alignment the voltage $u_{sd} = 0$ and assuming that R_s is small a simplification is made so that: $\Psi_{sq} = 0$ and the torque equation can be written as:

$$T_{el} = -p \frac{L_m}{L_r} (\Psi_{sd} i_{rq}) \quad (4.10)$$

Torque is thus controlled by controlling the q-part of the current flowing through the rotor. With a given torque reference T_{el}^* the current reference i_{rq}^* is given by:

$$i_{rq}^* = -\frac{L_r}{pL_m} \frac{T_{el}^*}{\Psi_{sd}} \quad (4.11)$$

Equation 4.11 is represented by block G_2 in figure 4.2

Reactive Current Control

The reactive power that is to be controlled originates in the stator windings. The reactive power is given by:

$$Q_s = u_{sd}i_{sq} - u_{sq}i_{sd} \quad (4.12)$$

Similarly to the torque current control equations it can be shown that the reactive current is controlled by the d-part of the rotor current. Using equation 4.3 and 4.5 the reactive power equation can be expressed as:

$$Q_s = u_{sd}i_{sq} - u_{sq}\left(\frac{\Psi_{sd} - L_m i_{rd}}{L_s}\right) \quad (4.13)$$

Again steady state condition is assumed which makes $u_{sd} = 0$ by definition. The reactive power equation can then be expressed as:

$$Q_s = -u_{sq}\left(\frac{\Psi_{sd} - L_m i_{rd}}{L_s}\right) \quad (4.14)$$

The reactive power is thereby controlled using the d-part of the rotor current. The reactive power is measurable and the current reference relating to reactive power can be controlled by a closed loop controller. The transfer function G_Q from Q_s to i_{rd} can be written as:

$$G_Q(s) = \frac{Q_s}{i_{rd} - \frac{\Psi_{sd}}{L_m}} = \frac{L_m}{L_s} u_{sq} \quad (4.15)$$

The control transfer function $F_Q(s)$ is chosen so that the closed loop system behaves like a first order transfer function which gives the following closed loop transfer function:

$$\frac{G_Q(s)F_Q(s)}{1 + G_Q(s)F_Q(s)} = \frac{\alpha}{s + \alpha} \quad (4.16)$$

The control transfer function is then:

$$F_Q(s) = \frac{\alpha}{sG_Q(s)} = \frac{\alpha L_s}{sL_m u_{sq}} \quad (4.17)$$

This is an integrator which means that no proportional control is needed. The α variable can be chosen. The control function $F_Q(s)$ is represented by block G_1 in figure 4.2.

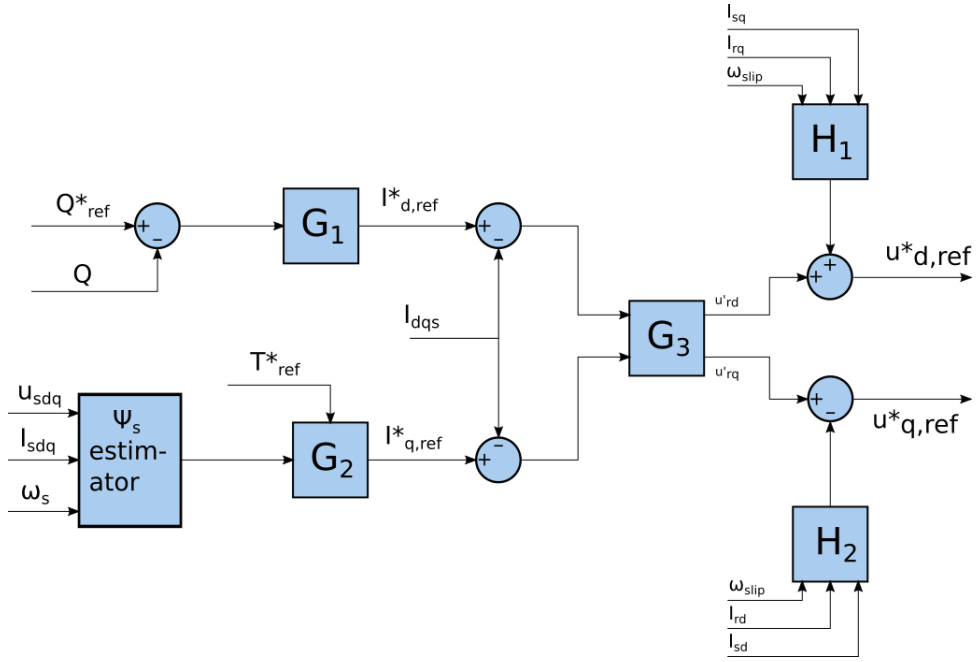


Figure 4.2: Rotor-side control system

Voltage Control

In order to achieve the desired currents a voltage needs to be applied over the rotor windings. This is achieved by applying a PI controller (G_3 in fig 4.2) to the current errors values. The output of the PI controller is defined from the rotor voltage equation 4.4 as:

$$e_r = i_r - i_r^* \quad (4.18)$$

$$u'_{rd} = k_{p,r} \left(e_{rd} + k_{i,r} \int e_{rd} dt \right) = \frac{d\Psi_{rd}}{dt} + R_r i_{rd} \quad (4.19)$$

$$u'_{rq} = k_{p,r} \left(e_{rq} + k_{i,r} \int e_{rq} dt \right) = \frac{d\Psi_{rq}}{dt} + R_r i_{rq} \quad (4.20)$$

The rotor reference values are then calculated by adding the remaining rotor voltage term as a feed forward using actual values measured from the system. This is done to ensure better tracking.

$$u_{rd}^* = u'_{rd} + (\omega_s - \omega_r)(L_m i_{qs} + L_r i_{qr}) \quad (4.21)$$

$$u_{rq}^* = u'_{rq} - (\omega_s - \omega_r)(L_m i_{ds} + L_r i_{dr}) \quad (4.22)$$

The feed forward functions are represented by H_1 and H_2 in figure 4.2. The voltage references are finally converted back into three phase values by applying the inverse Park transform and the appropriate voltages are output by the RSC.

4.2.2 Grid-side Converter Control

The grid-side converter (GSC) control system has a similar structure compared to the RSC but it is somewhat simpler. The main job of the controller is to balance the power

flow from the grid to the rotor. If the RSC is pulling power from the DC-link the same amount of power needs to flow in to the DC-link from the grid to ensure that the voltage over the DC-link capacitor remains constant. The relationship between power flow and DC-link voltage means that controlling the DC-link voltage to be constant automatically controls the power flow to be balanced. This is what is exploited in the GSC control. Additionally the GSC can compensate for or inject reactive power on the grid. The control algorithm is represented by figure 4.4 which parts are explained in the following section. The GSC is connected to the grid via an RL-filter and the equivalent circuit representation can be seen in figure 4.3.

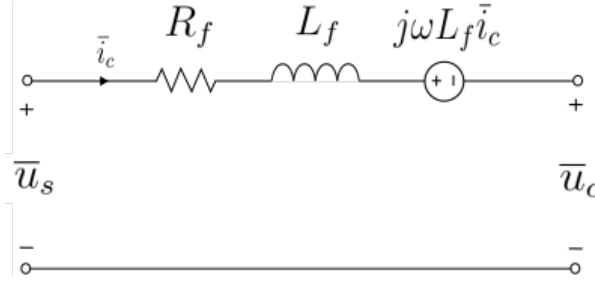


Figure 4.3: Equivalent circuit representation of RL filter connecting the GSC to the grid

The grid voltage vector is the same as that of the stator voltage and will be referred to as \bar{u}_s . The filter consists of resistive components (R_f) and inductive components (L_f) the GSC voltage \bar{u}_c equations are given as:

$$u_{cd} = -R_f i_{cd} - L_f \frac{di_{cd}}{dt} + \omega L_f i_{cq} \quad (4.23)$$

$$u_{cq} = u_{sq} - R_f i_{cq} - L_f \frac{di_{cq}}{dt} - \omega L_f i_{cd} \quad (4.24)$$

The reference frame is again aligned with the grid voltage vector \bar{u}_s , aligning the voltage vector with the q-axis which allows the active and reactive power to be controlled independently by controlling the q or d part of the current. This follows from the fact that active and reactive power injected or pulled from the grid is given by:

$$P_{active} = u_{sq} i_{cq} \quad (4.25)$$

$$Q_{reactive} = -u_{sq} i_{cd} \quad (4.26)$$

Thus the d-part of the current controls reactive power and the q-part control active power.

As mentioned previously the power flow is controlled by controlling the DC-link voltage. Due to the nature of active and reactive power it follows that in order to charge or discharge the DC-link capacitor active power needs to be injected or withdrawn. The active power control is executed by a PI controller working with a DC voltage reference. The output of the PI controller is defined as the q-part of the current reference i_{cq}^* . This is represented by block C_2 in figure 4.4.

The reactive power is likewise controlled by a PI controller (C_1 fig 4.4) with a reactive power reference value, in this work the reactive power reference was set to zero. The

resulting PI output is regarded as the d-part current reference i_{cd}^* .

The acquired current references are used in a third PI controller (C_3 in fig 4.2) whose output is defined from the voltage equations as:

$$e_c = i_c^* - i_c \quad (4.27)$$

$$u'_{cd} = k_{p,g} \left(e_{cd} + k_{i,g} \int e_{cd} dt \right) = R_f i_{cd} + L_f \frac{di_{cd}}{dt} \quad (4.28)$$

$$u'_{cq} = k_{p,g} \left(e_{cq} + k_{i,g} \int e_{cq} dt \right) = R_f i_{cq} + L_f \frac{di_{cq}}{dt} \quad (4.29)$$

Similarly to the RSC the remaining components of the voltage vector are then added as a feed forward function to get the voltage reference values:

$$u_{cd}^* = -u'_{cd} - \omega_s L_f i_{cq} + u_{sd} \quad (4.30)$$

$$u_{cq}^* = -u'_{cq} + \omega_s L_f i_{cd} + u_{sq} \quad (4.31)$$

The feed forward functions are represented by by the D_1 and D_2 blocks in figure 4.4.

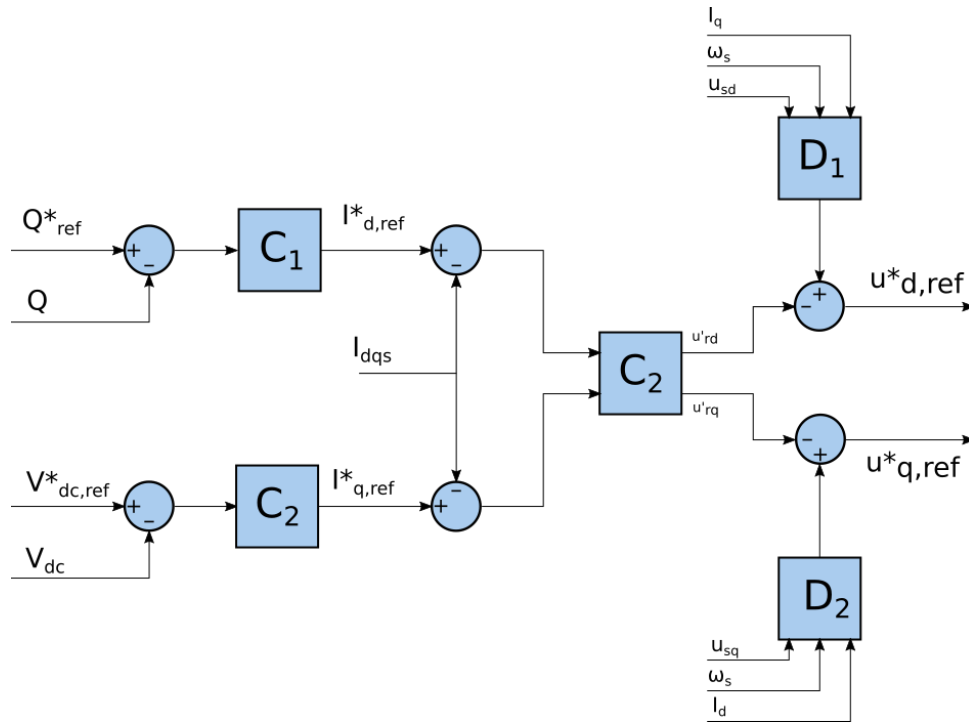


Figure 4.4: Grid-side control system

4.3 Speed Control Scheme

The ability to control the speed of the generator has one main advantage. Altering the engine speed affects the hot-side temperature which is controlled by engine pressure. Therefore the required engine pressure in order to keep the temperature at a certain value is altered. The engine pressure in turn affects the efficiency of the system as efficiency depends on engine pressure and temperature as shown in section 3.2.1. As a result the system efficiency can be optimized by altering the speed of the engine. Additionally speed control can work as a safeguard to overheating which otherwise can be devastating for the system. Figure 4.5 shows the flowchart representing the speed control algorithm that was developed. The torque control block is the RSC control system discussed in a previous section. The system pressure is controlled by the temperature controller, the temperature control is a company secret and will not be discussed further. The optimizing speed control is done by a series of PI controllers and is described in the following section.

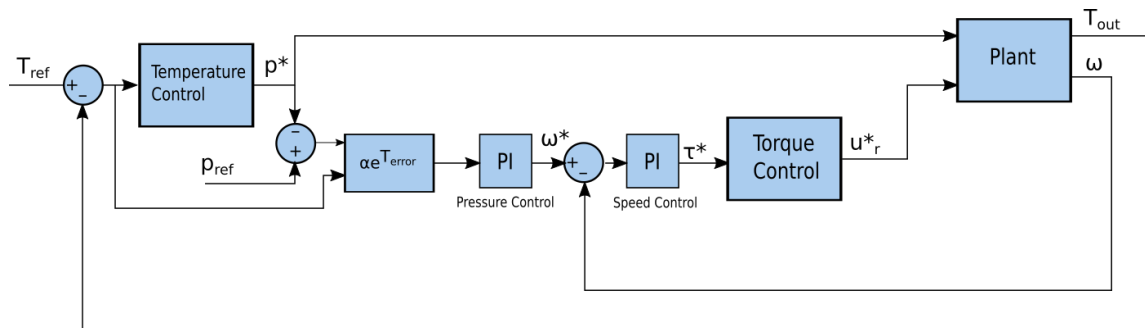


Figure 4.5: Flowchart of temperature and speed control system

The challenge with controlling the speed to achieve a certain pressure is that that the speed does not control pressure directly, it controls temperature. The temperature controller however does control the pressure. Technically it could be possible to operate the system with a constant pressure and do all temperature control with the help of the speed controller. However there are limitations to speed control in the responsiveness and range of the controller. In this configuration there are essentially two controllers that control temperature with different outcomes in mind which can lead to oscillations and poor control of the system. There are several possible solutions to solve this problem, one could for example be to overhaul the entire control system to integrate the added dynamics of speed control in a comprehensive control algorithm. That solution is not an option in this work and a second approach has been adopted: prioritization of controllers depending on the situation.

Three situations were identified as significant:

1. Achieving reference temperature
2. Operating at reference temperature
3. Overshooting reference temperature

In situation one the most important factor is that the system achieves the reference temperature in order for the system to function properly and effectively. This is most safely done by controlling the pressure of the system. In situation two the system is

operating at the desired temperature, however the efficiency can still be increased by controlling the speed of the system. In situation three it is important that the temperature does not overshoot too much, in optimal operation the pressure will already be maximized in this situation which means that the speed control will have to be applied.

The prioritization can be done in different ways as well. It could for example be done by switching between controllers or running the two controllers at different bandwidths. However a very simple method was found that had satisfying results. By observing that the speed control is less significant in situation one, more significant in situation two and extremely significant in situation three and that these situations correspond to the temperature error factor being positive, zero and negative a solution was devised. The pressure error used by the speed controller is simply multiplied with the negative exponential of the temperature error: $\beta e^{-(T^*-T)}$, the result is that speed control is reduced in situation one, unaffected in situation two and amplified in situation three. The factor β is chosen to control the significance of amplification factor. This method results in the temperature control being dominant when the system is achieving the reference temperature and the speed controller being dominant when the system is overheating. In the middle where the system is working in the reference temperature range both controllers output moderate control signals which result in increased engine pressure while keeping the reference temperature constant. The reason why this is preferred over the other options is that the speed controller and temperature controller need to work together in order to increase pressure while keeping the temperature constant.

4.4 Hybrid Control

In hybrid operation the system operates with two power sources: the sun and an additional gas burner. The challenge with developing a controller for the burner operation is the possibility of overheating the system. For example if the irradiance is reduced due to cloud coverage the system will start burning fuel to achieve full power generation. If the sun suddenly comes out of the clouds the system suddenly has more power coming in than it can handle. It is also important that the temperature does not overshoot when the controller ramps up the power in the first place.

A very simple controller was chosen at this stage due to insecurity in the models temperature dynamics. A relatively slow PI controller was used with the control reference being produced power. If the temperature overshoots a feed forward was used to rapidly reduce the gas flow.

4.5 APF control

The APF functions in this work was designed to compensate for reactive power. The control used was completely identical to that of the grid-side controller discussed in section 4.2.2.

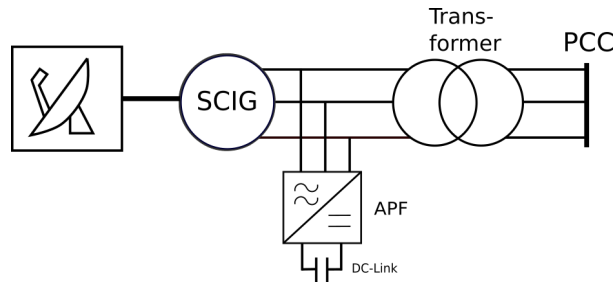


Figure 4.6: Configuration of SCIG with APF

Figure 4.6 shows how the APF system configuration. When working with several Dish-Stirling systems the APF could be connected at a common coupling point, compensating for all consumed reactive power at the same time. The advantage of using an APF instead of a passive filter is that more services like harmonic compensation are enabled. In addition a load or BSS can be connected to the DC-link allowing for a more complex and versatile system.

4.6 Electrolyser Model

The modeling of the electrolyser is based on the model presented in the work of Ursúa and Sanchis [33]. The paper presents a detailed static-dynamic model of an alkaline electrolyser. The model represents one electrolytic cell and is configured to represent an electrolyser by modeling several cells in series. The model used in this work is closely in line with the model represented in the for mentioned paper and all equations are derived from that work but the number of cells is adjusted to represent an electrolyser with a different power consumption. See appendix A for equations.

The equations were applied in a model developed in MATLAB Simulink. The resulting model was then integrated with the DFIG and SCIG with APF models. The electrolyser was connected to a DC-DC converter that was connected the DC link of the systems, the configuration can be seen in figures 4.7 and 4.8. The DC-DC converter was modeled by a voltage source so current harmonics related to a switching converter were not present. The DC-DC converter was controlled as a current source for the electrolyzer and the electrolyser was only turned on when optimal operation conditions could be achieved, meaning that the system could supply a current of 120A.

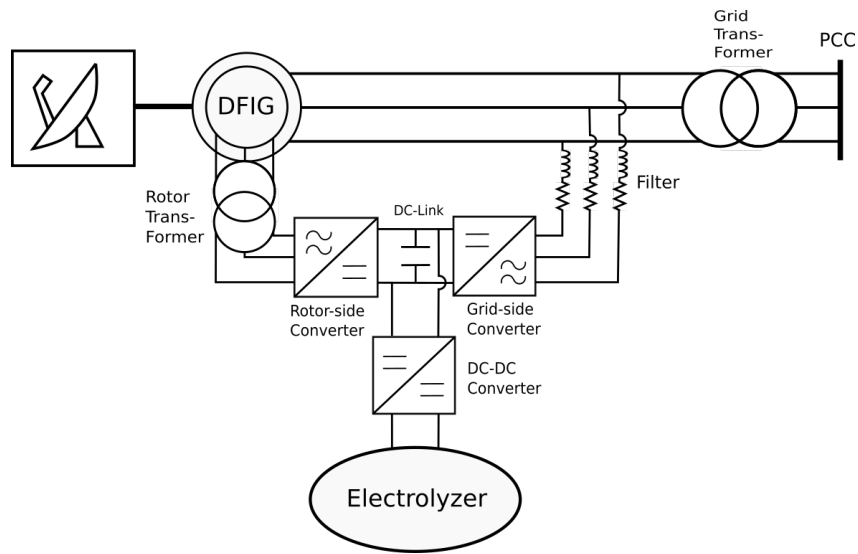


Figure 4.7: DFIG system with electrolyser

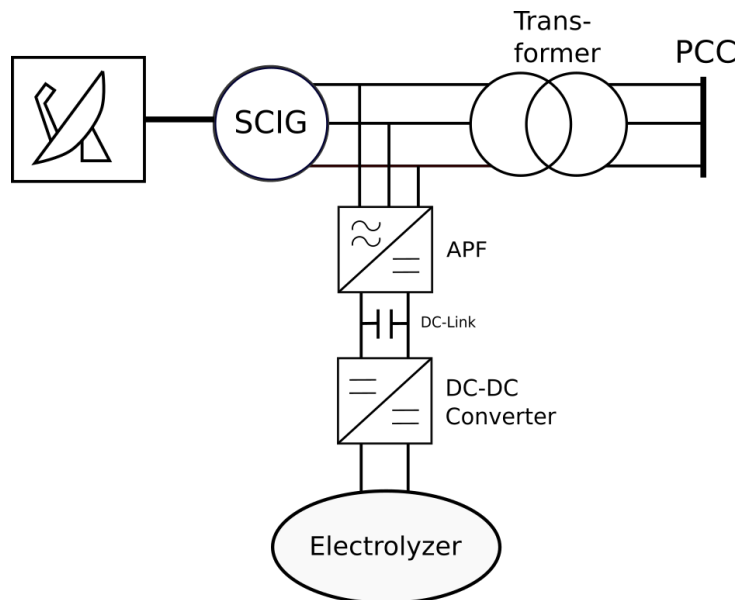


Figure 4.8: SCIG system with APF and electrolyser

Chapter 5

Results

5.1 System Performance

It should be emphasized that the model presented in this thesis has not been validated with the actual system and the results should therefore not be seen as predictions but instead as indications. Simplifications have been made and it is difficult to know how these affect the end result before validation. The system has been tested against the data presented in Lopez et.al [14] to verify how well the model follows the base input conditions. As can be seen in figure (5.1) the model follows the real values very well.

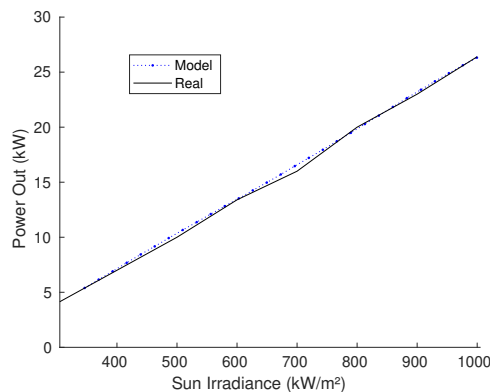
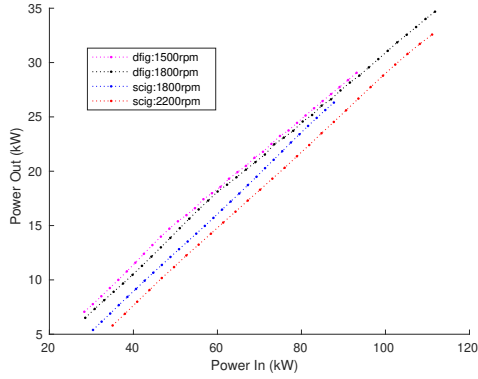


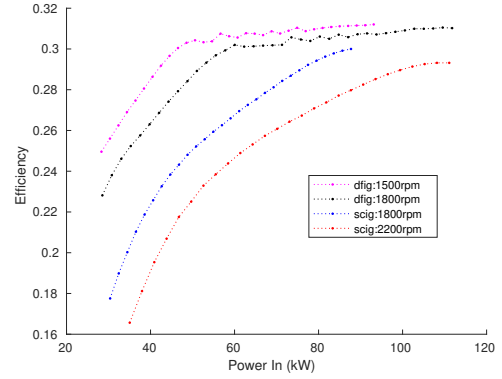
Figure 5.1: Model power output compared to real values

The Stirlingversal system uses a dish with a projected area of $105m^2$, maximum pressure of $220bar$ and working a temperature of $700^{\circ}C$. The Stirling engine has higher efficiency the higher the engine pressure is as shown in section 3.2.1. The Stirling engine's two driving axles are connected to the generator via cogwheels. The relation between the generator's nominal rotor speed and the engine's nominal speed can therefore be chosen. By having a lower nominal engine speed the engine will require a higher pressure in order to extract the incoming energy, which should result in a higher efficiency at lower power levels but reduce the overall power range. By increasing the nominal speed of the engine the efficiency will decrease but the range will increase because at the highest engine pressure more energy can be extracted from the receiver. The system was therefore simulated in four different configurations in order to compare the resultant effects on power generation, range and efficiency. The results are presented in figures 5.2 and 5.3:

- SCIG:1800rpm; SCIG configuration with nominal engine speed of 1800rpm
- SCIG:2200rpm; SCIG configuration with nominal engine speed of 2200rpm
- DFIG:1500rpm; DFIG configuration with nominal engine speed of 1500rpm
- DFIG:1800rpm; DFIG configuration with nominal engine speed of 1800rpm

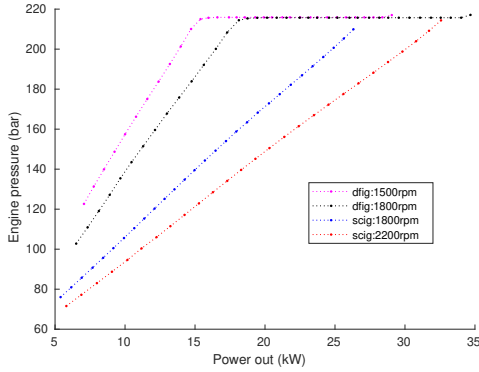


(a) Output power over power input range

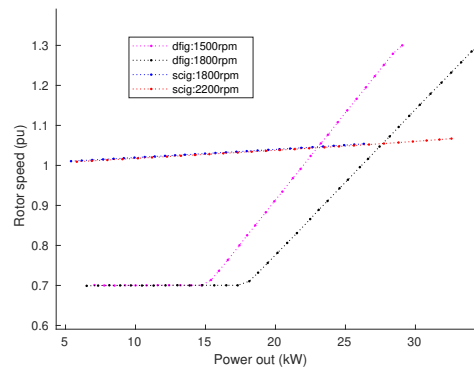


(b) Efficiency over power input range

Figure 5.2: System output power and efficiency



(a) Engine cold-side pressure over power output range



(b) Rotor speed over power output range

Figure 5.3: System pressure and rotor speed performance

From figure 5.2b it is concluded that the higher the nominal speed of the Stirling engine is, the lower the overall efficiency becomes. The DFIG systems show a higher peak efficiency which is due to the DFIG being more efficient than the SCIG. Figure 5.2a shows that a higher nominal engine speed gives the system a higher peak output power: the 1800rpm SCIG system does not have the range to achieve 30kW power extraction while the 2200rpm version exceeds 30kW. An optimal nominal engine speed could be found for both the SCIG and DFIG system to make the maximum power extraction the target of 30kW which in turn would increase efficiency at lower power levels.

Both DFIGs have superior efficiency, especially in the lower regions of incoming power. At around 50kW incoming power maximum engine pressure is reached, at this point the system generates around 15kW. Due to its higher nominal speed the 1800rpm DFIG version is able to achieve higher peak power extraction. Comparing the DFIG efficiency curves with figure 5.3b and 5.3a it is observed that the engine pressure has a strong effect on system efficiency. It can also be seen that rotor speed has a small effect on the efficiency of the system. The 1800rpm system has a high output capability and at the higher output levels very similar efficiency compared to the 1500rpm system. This configuration is chosen as the optimal DFIG configuration and further DFIG simulations are done with that system only. The 2200rpm SCIG configuration is likewise chosen for further experiments due to its wider range. Since the proposed system obtains energy from both the solar irradiation and fuel burner it follows that fuel consumption is directly dependent on incident irradiance. Figure 5.4 shows the amount of fuel required in order to generate 30kW of electricity depending on the sun irradiance level.

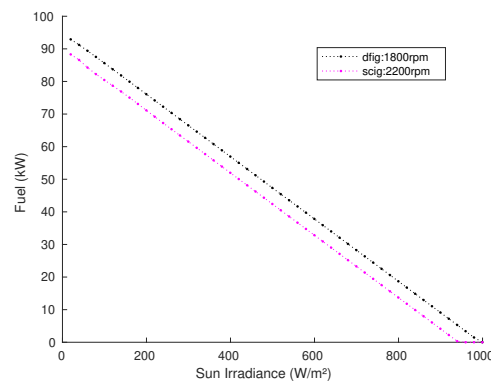


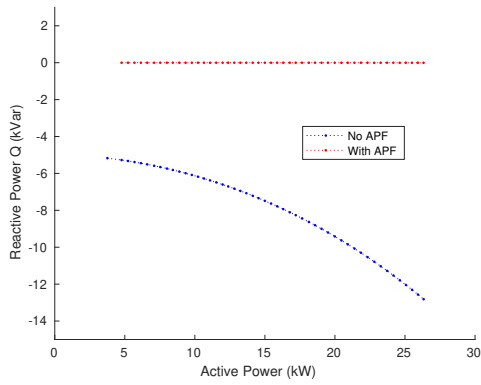
Figure 5.4: Fuel consumption at 30kW output power compared to irradiance

It can be observed that the DFIG configuration consistently requires less fuel. This difference is a result of that the SCIG configuration has not reached maximum pressure when producing 30kW as well as the slightly higher efficiency of the DFIG generator. If the nominal speed of the SCIG system was optimized the fuel consumption would be even more similar.

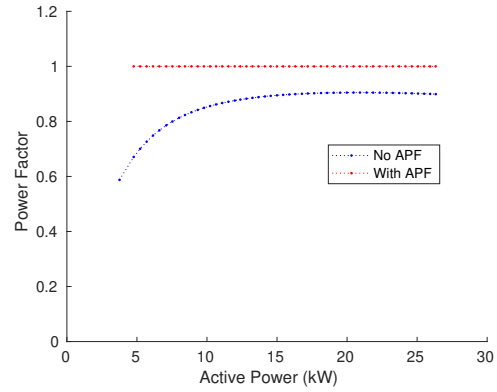
5.2 Power Quality & Power Flow

In order to ensure that no reactive power is consumed from the grid by the SCIG an APF is installed. The APF is controlled to compensate for all reactive power consumed by the generator. The result can be seen in figure (5.5a), the APF manages to reduce the reactive power to zero at all levels of generated power. The Resultant power factor before and after APF can be seen in figure (5.5b). As can be seen the APF compensates for all reactive power. In the DFIG, reactive power compensation is achieved through the control of the rotor currents. The reactive power of compensation result of the DFIG was found to be the same as for the APF: no reactive power was consumed from the grid.

When designing a system with power converters a key aspect of the system is the required power capacity of the converter. The simulated power flow through the converters



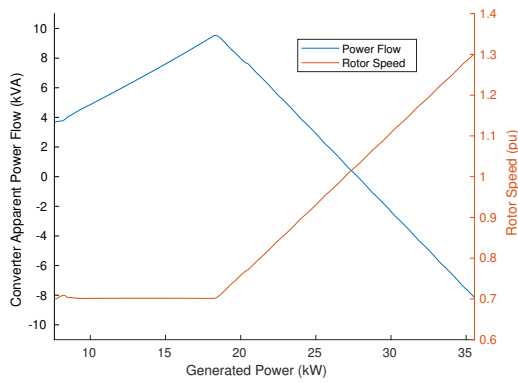
(a) Active power vs reactive power, with and without APF



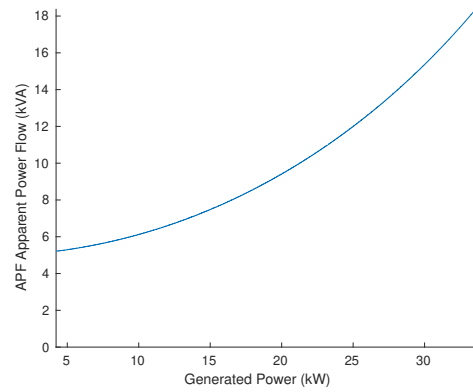
(b) Power factor with and without APF

Figure 5.5: Reactive power with and without PQI

as a result of the developed control algorithms can be seen in figure 5.6b for the APF and figure 5.6a for the DFIG. The figures show the apparent power flowing through the converters as a function of the power output of the system. According to these results the required converter capacity for the DFIG system is around 9.5×2 kW. The APF would require a 19kW converter if operated at maximum power. Note that the DFIG has two converters where the APF only requires one. The results show that an APF filter requires a converter with similar power capacity as the total capacity of the DFIG converters to achieve a power factor of one. It can also be seen that the power flow through the DFIG converters relate to power generation and rotor speed. When the generator operates at sub-synchronous speed the power flow is positive, at super-synchronous speed the power flow is negative.



(a) Power flow through GSC and RSC of the DFIG over power generation range



(b) Power flow through the APF over power generation range

Figure 5.6: Converter power flow, reactive power compensation

5.3 Electrolyser Result

The electrolyser is assumed to be working at a temperature of 50°C with energy supplied by the waste water heat produced by the system. Figure 5.7 shows the resulting I-V characteristics obtained from the implemented model and those presented in the article Ursua et.al [33] from which the model is derived. The simulation follows the presented values quite well. When the current approaches zero the result gets less accurate but this is not deemed consequential.

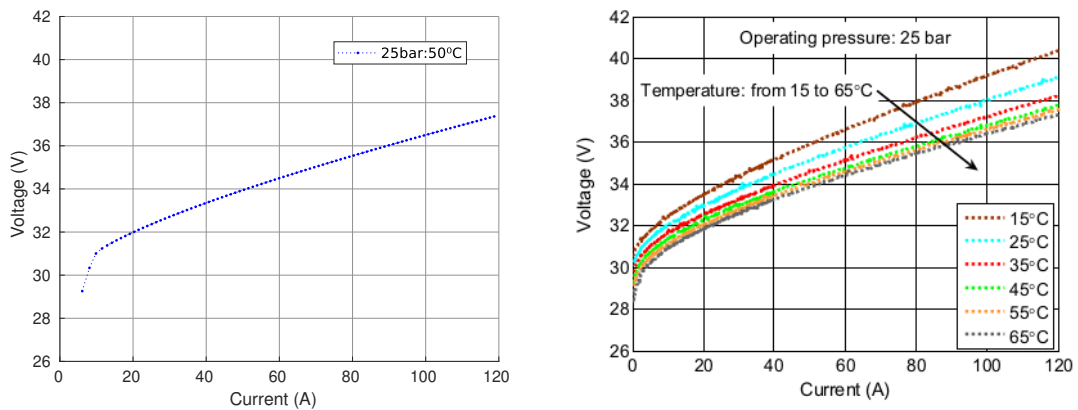
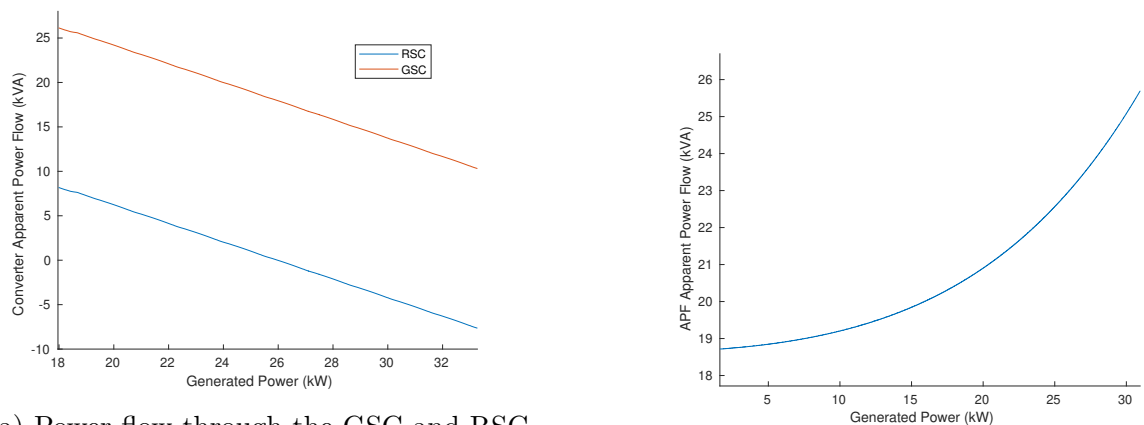


Figure 5.7: Model IV graph and reference IV graph [33]

The electrolyser implemented in the model comprises of 88 cells in the stack, which result in a 18kW electrolyser. If the electrolyser is connected to the system via the DC-link the power converters need to be able to supply enough power to drive it. In addition they need to be able to compensate for reactive power at the same time. The power flowing through each power converter is therefore measured and the minimum size requirement is estimated.



(a) Power flow through the GSC and RSC of the DFIG system when the electrolyser is turned on

(b) Power flow through AFP converter when the electrolyser is turned on

Figure 5.8: Converter power flow with electrolyser

The APF handles reactive power during normal operation. The addition of an electrolyzer means an added demand of active power flowing through the converter. The resulting power requirement of the converter will be the apparent power that is a combination of both. It can be seen in figure 5.6b that the converter only needs a 6kW increase in capacity in order to supply the 18kW electrolyser with active power. In the case of the DFIG the GSC already injects or absorbs active power in normal operation, however, it can be seen that the power flow of the RSC will have an impact on converter size requirement. At sub-synchronous speed the GSC supplies power for the electrolyser and the rotor, at super-synchronous speeds however power flows out of the rotor supplying the electrolyser with power, in turn requiring the GSC to transfer less energy. If the electrolyser is only used when maximum power generation is achieved the power flows from both the grid and the rotor to the electrolyser. In this case a very slight increase in converter capacity will be required. However if the electrolyser is activated when just enough power is generated by the system the GSC capacity will have to be increased significantly.

Chapter 6

Energy System Comparison

6.1 System Definition

To be able to compare a hybrid Dish-Stirling system with another system it is important to establish what the systems are capable of and if they are comparable. A hybrid Dish-Stirling system runs on solar power and a secondary resource in the form of gas. The system is able to reliably produce energy all hours of the day regardless of the weather conditions. The most natural comparison would be with a PV based system, PV panels by themselves are not able to produce energy at all times of the day however, so some form of energy storage is needed in order to make the systems comparable. It should be noted that, even with energy storage, the PV cannot guarantee meeting the energy demand if solar irradiation is lacking for a longer amount of time. The visual representation of the two systems can be seen in figure 6.1.

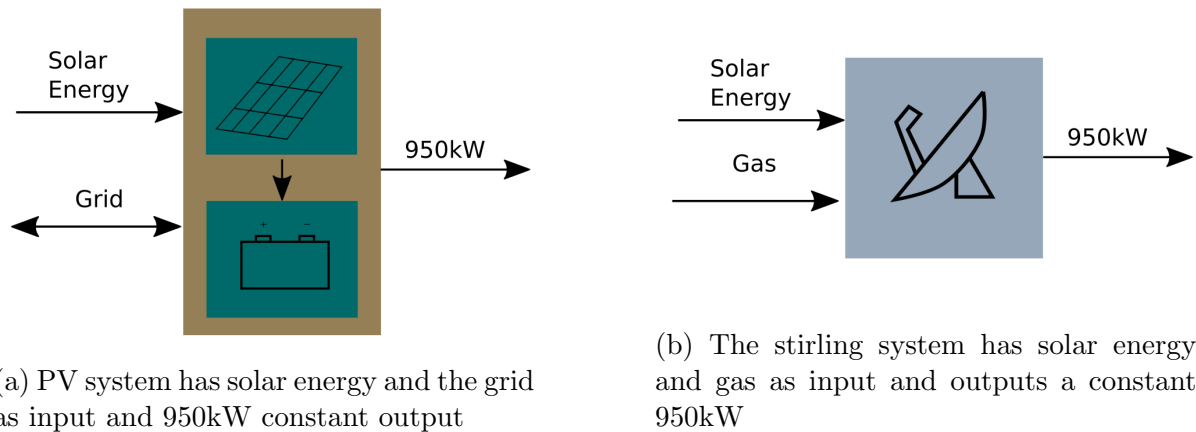


Figure 6.1: Visual representation of the systems considered in the comparison

The scenario that is used for this comparison is a futuristic fueling station where customers can charge their electric vehicles and fuel their hydrogen based vehicles. Hydrogen is produced on-site with an electrolyser which is powered by the energy system. The electric energy demand is defined as 950kW, some of that would be used to charge cars and some would be used in electrolysis to make hydrogen fuel. Only the energy generation of the systems is considered for comparison because the electrolysis system, hydrogen storage and other such hardware costs are considered to be similar between the

two systems. Since at least an important fraction of the energy required is expected to come from the sun, the physical location of the fueling station will have a large impact on the system size and cost. Two locations are chosen for comparison, one with less favorable solar conditions (Lund, Sweden) and one with more favorable conditions (Johannesburg, South Africa).

The PV system will need to be able to generate enough power during the sunny hours of the day to be able to supply the fueling station with energy during the night. A battery large enough to store all the energy needed during the night needs to be installed. If the system is to be able to produce power over the whole year it needs to be designed considering the conditions of the least sunny month of the year.

The PV power generation is calculated by the method presented in Huld et.al [34]:

$$P(G', T') = G'(P_{STC}, mk_1 \ln(G') + k_2 \ln(G')^2 k_3 T' + k_4 T' \ln(G') + k_5 T' \ln(G')^2 k_6 T'^2) \quad (6.1)$$

Where $G' = G/G_{STC}$ and $T' = T - T_{STC}$. G is in-plane irradiance and T is temperature, STC stands for *standard test conditions*, $G_{STC} = 1000W/m^2$ and $T_{STC} = 25^\circ C$. The temperature was assumed to be a constant $25^\circ C$ because ambient temperature is not taken into account for the Dish-Stirling system. The constants are set to the same as presented in the paper. Monthly average solar irradiation profiles were acquired from [35] and used as input data for the simulation. The amount of modules required by the PV system is chosen as the least amount of modules needed to produce enough excess energy during the day to supply the energy demand during the night. The requirement is modified by the round-trip efficiency of the battery and other system losses.

Battery lifetime is highly dependent on the use: charging/discharging currents, depth of discharge and temperature. To calculate required battery size for 10 years of operation a model presented in Motapon et.al [23] was used:

$$N_c(n) = N_{c,ref} \left(\frac{DoD(n)}{DoD_{ref}} \right)^{\frac{-1}{\epsilon}} \left(\frac{I_{dis,ave}(n)}{I_{dis,ref}} \right)^{\frac{-1}{\gamma_1}} \left(\frac{I_{ch,ave}(n)}{I_{ch,ref}} \right)^{\frac{-1}{\gamma_2}} \quad (6.2)$$

It is assumed that a temperature control system is in place and therefore the temperature factor is omitted from the original model. One cycle per day is assumed with charging and discharging currents being the average currents flowing in and out of the battery during the day. The constants are acquired from the model presented in the paper and the battery is assumed to be of LFP type. The maximum battery lifetime is considered to be 10 years. The stirling dish fuel consumption is calculated with the results shown in figure 5.4.

6.1.1 Location: Lund, Sweden

Lund is situated quite far up in the northern hemisphere, as a result winter days are short and dark while summer days are long. This results in more solar panels or Dish-Stirling units having to be installed in order to generate enough solar power to meet energy demand. In the case of the Dish-Stirling system it means that if hybrid mode is not activated a unit is working at lower power input levels.

PV system specifications

Because of the solar conditions it is impractical to design a PV system that can generate enough energy during the winter as this would require 52.64MWp solar panel capacity. Instead the system is designed to produce enough energy for half the year and import energy from the grid during the winter. Costs associated with grid connection are hard to estimate since different locations have differing conditions when it comes to proximity to an existing grid and other installation difficulties. The average in-plane global horizontal irradiance (GHI) on a day in September can be seen in figure 6.2a, and the resulting PV power generation in figure 6.2b. The required battery size to service the entire night is quite large, the upside of that is that the battery has low charging and discharging currents as a result. In turn that allows a battery life of 10 years at a DoD of 0 - 100% according to [23].

PV	Value	Battery	Value
Installed capacity	7.26MWp	Size	14.7MWh
Module efficiency	20%	Round-trip efficiency	88%
System losses	14%	Lifetime	10 yrs
Mounting	Fixed	Technology	Li-ion

Table 6.1: Lund PV system specifications

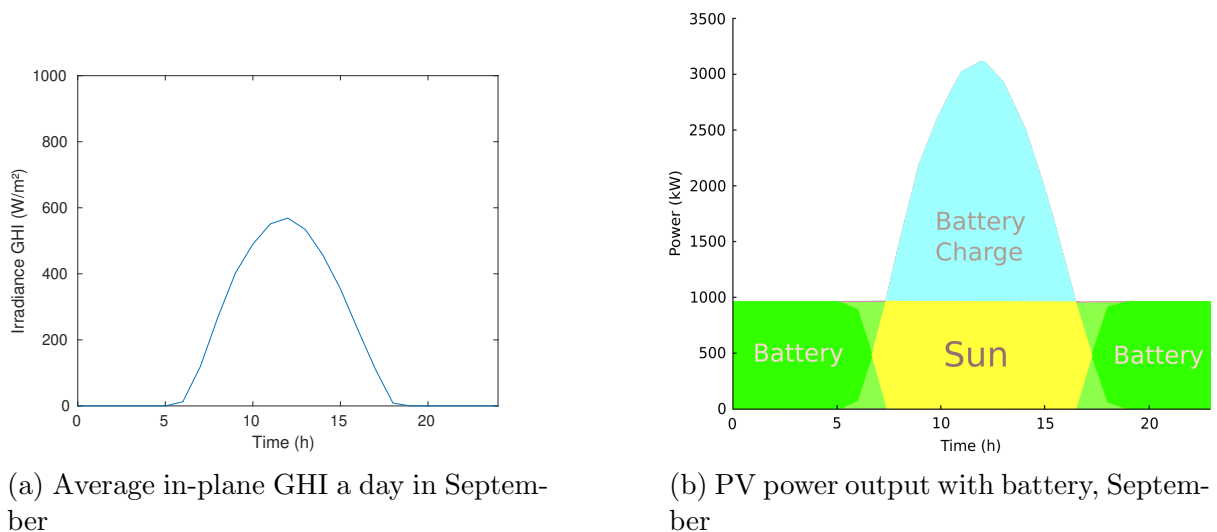


Figure 6.2: Average in-plane GHI profile PV power output, Lund

The system would be dimensioned to deliver 950kW continuously over the day. This power level would allow 5-10 electric cars charging at full power simultaneously at all hours of the day and produce enough hydrogen to supply three hydrogen cars with 3kg H_2 per hour (enough to transport a mid-sized car a distance of 300km). The proposed system produces a large amount of energy which is reflected by the required PV capacity. The area of that amount of solar panels would be around 36,000 m^2 . The required BSS is also quite large, it corresponds to around 150 of the Tesla model S largest batteries put together or 15 standard 40 feet battery containers.

Dish-Stirling System Specifications

The Dish-Stirling hybrid system is considered with the SCIG 2200rpm configuration and the DFIG 1800rpm configuration. The study considers two system configurations, the first configuration features the least amount of units needed (33) to meet the power demand. In this configuration all units need to be operated at constant full power which would maximize the utilization of the hardware. Then a configuration featuring three times as many units is considered. In that case the energy mix will have a larger contribution of solar energy and consume less gas. The dish area of each unit is $105m^2$, giving the two system versions a total area of approximately $3500m^2$ and $10,500m^2$ respectively. The plant is controlled so that it generates at least 950kW at all hours of the day. The fuel consumption calculations are made from average insolation data hourly. The units working in hybrid operation are set to produce 30kW, the units that are not in hybrid-mode use solar power only. Every hour it is evaluated how many units need to be in hybrid-mode to reach the power demand and the amount of fuel they consume. The irradiance profile that is used with the stirling dish system is direct normal irradiance (DNI). The average DNI in Lund a day in July can be seen in figure 6.3a and the resulting hybrid power generation can be seen in figure 6.3b.

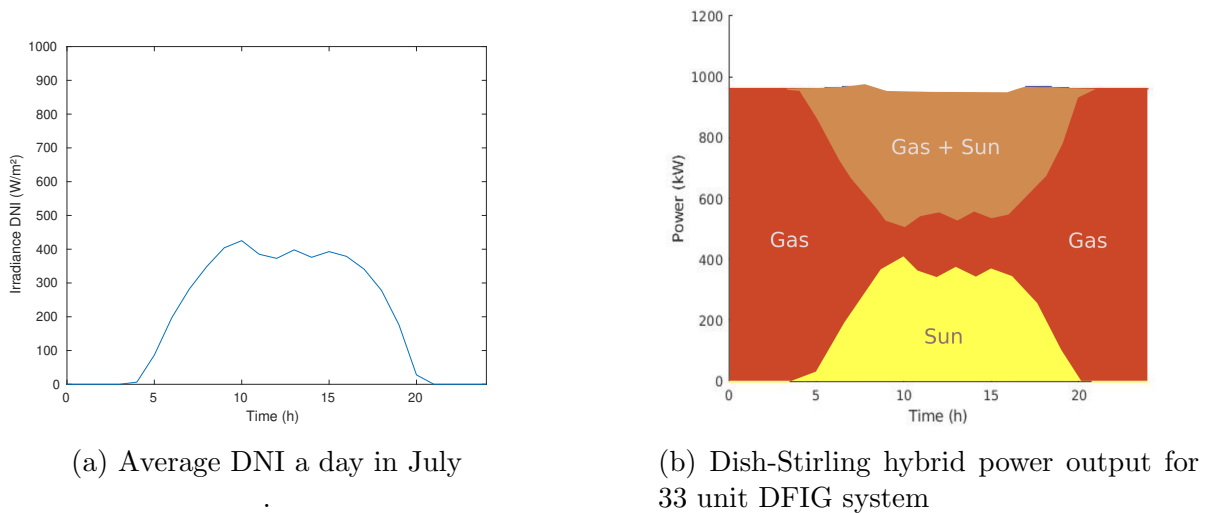


Figure 6.3: Average DNI profile and Dish-Stirling power generation, Lund

As can be seen, the Dish-Stirling system produces most of its energy from gas with this configuration. The energy source mix over the year can be seen in figure 6.4a. The result shows that there is very little difference when it comes to the energy mix between the two configurations. Figure 6.4b shows the amount of gas consumed every month of the year, due to the low insolation and low number of Dish-Stirling units the gas consumption is only slightly decreased during the summer months. The gas consumption over one year comes to 22,100MWh for the DFIG system and 23,483MWh for the SCIG system, that is 6.3% more fuel consumed by the SCIG system.

The energy mix and gas consumption can be improved by installing more Dish-Stirling units, utilizing more of the solar energy. This increases the initial investment but decreases the amount of gas needed over the year and it gives the system a three times

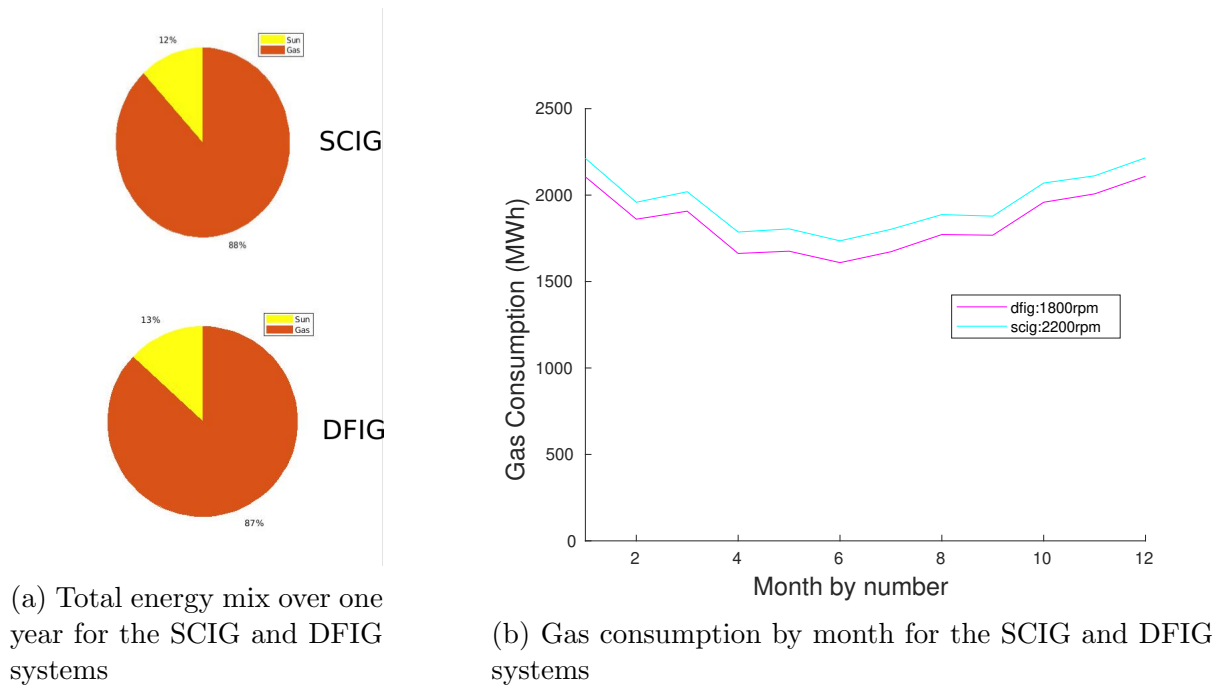


Figure 6.4: Energy mix and gas consumption, 33 unit systems, Lund

higher peak energy generation capability. Figure 6.5 shows the 99 unit configurations' resulting energy mix. In the new configuration, the system is able to reduce gas consumption significantly during the summer months. It is also observed that the DFIG system outperforms the SCIG system in this scenario. That is because more of the units work in non-hybrid mode at energy levels where the DFIG system is more efficient. The resulting gas consumption for one year is 17,882MWh for DFIG and 20,814MWh for SCIG. The

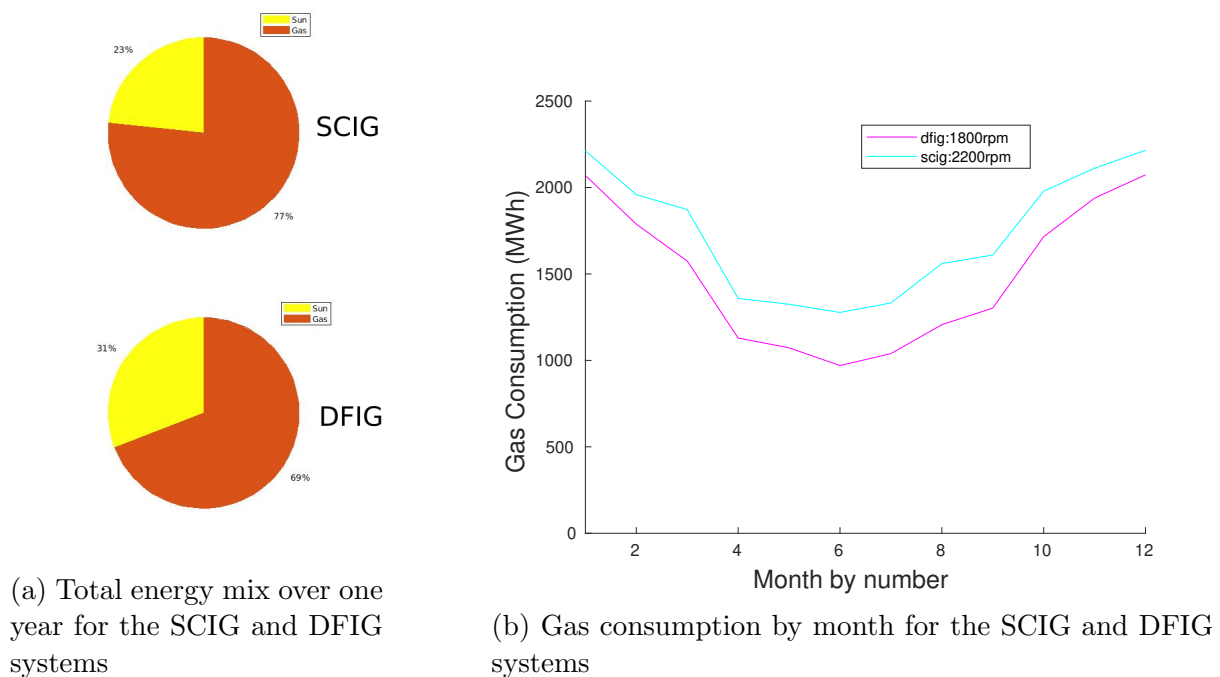


Figure 6.5: Energy mix and gas consumption, 99 unit system, Lund

SCIG system now consumes 16.4% more fuel.

Figure 6.6 shows the total power produced by PV; represented by the blue line and the Dish-Stirling systems; represented by the orange line. The figure displays data from the 33 unit system, the 99 unit system has the same energy output but differ in the gas consumption as can be seen in figure 6.5. The PV system produce more energy than is consumed during the summer months and less energy than is consumed during the winter. This is solved by selling excess energy to the grid during summer and buying energy from the grid during winter. If for some reason the grid was not an option there would have to be a separate energy source that could produce the required energy in the winter.

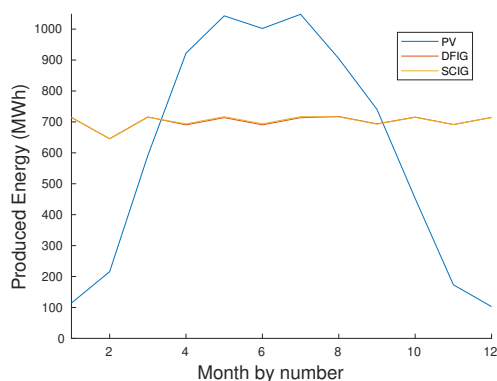


Figure 6.6: Energy output over one year 33 units, Lund. A similar result is found for the 99 unit system

Cost Comparison

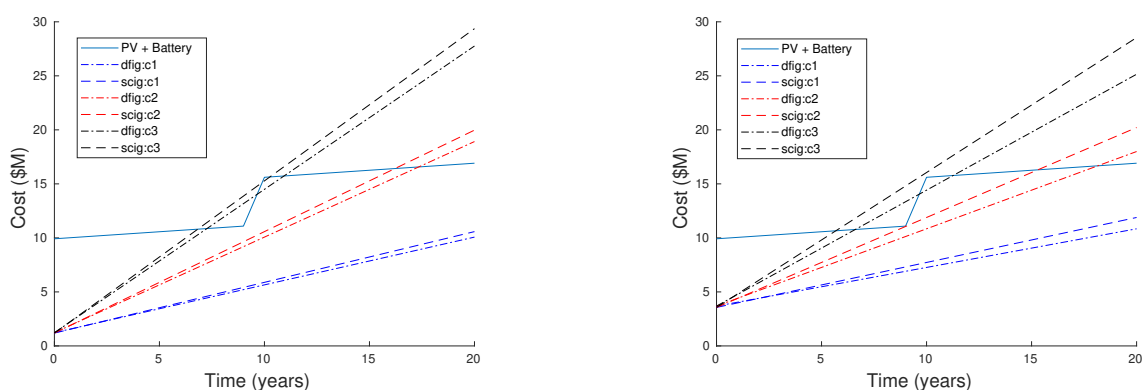
Cost is of course an important factor to consider when it comes to judging the viability of the system. The cost calculations have been based on the cost assumptions presented in table 6.2.

Component	Cost	Consumable	Value
PV system	\$700/kWp	Gas c1	\$0.02/kWh
Li-ion Battery-pack	\$300/kWh	Gas c2	\$0.04/kWh
Stirling SCIG System	\$1200/kWp	Gas c3	\$0.06/kWh
Stirling DFIG System	\$1255/kWp	Electricity buy	\$0.08/kWh
Grid cost	10%	Electricity sell	\$0.04/kWh

Table 6.2: Cost values used in the comparison of PV and Dish-Stirling systems

The PV system cost is the cost for a complete installation of a PV system including modules, engineering, inverter and work costs, the data is acquired from [36]. The same is included in the Dish-Stirling cost which is acquired from Stirlingversal. The DFIG and converter cost is loosely based on figures in [37], the assumed costs are higher compared to the reference in order to take into account increased costs associated with a smaller scale production. The converter cost is estimated to \$40/kW. The DFIG system was

found to require around 19kW converter capacity. The generator cost for the SCIG is estimated as \$60/kW and the DFIG cost is assumed to be 50% higher, the estimation is assumed to be on the high side. The SCIG system considered here is the cheapest possible system configuration, no APF is used and reactive power can therefore not be controlled. The Li-ion battery cost only regards the the battery-pack, no installation or containment costs are considered, this is because no gas containment cost is taken into consideration. The battery cost is acquired from [22]. It is hard to estimate an exact gas cost because of fluctuating prices, taxes and the unconventional sources that can be utilized, therefore three different gas costs are considered. Electricity cost is a mean yearly estimate and does not consider seasonal changes. The selling price for electricity is assumed to be half of the buying price. The cost comparison over 20 years can be seen in figure 6.7 and individual costs can be seen in table 6.2.



(a) Costs over 20 years, 33 unit systems vs PV

(b) Costs over 20 years, 99 unit systems vs PV

Figure 6.7: Project system cost over 20 years, Lund. Three gas costs are considered: c1, c2, c3 which can be seen in table 6.2

Cost Table: Lund						
Thing	33 Unit System			99 Unit System		
Gas cost (\$/kWh)	0.02	0.04	0.06	0.02	0.04	0.06
SCIG						
CAPEX (\$/kWh)	1.19			3.57		
OPEX (\$M/year)	0.47	0.94	1.41	0.4	0.8	1.2
Total Cost (\$M)	10.6	20	29.4	11.9	20.2	28.5
Break even (\$/kWh)	0.0335			0.0321		
DFIG						
CAPEX (\$/kWh)	1.24			3.73		
OPEX (\$M/year)	0.44	0.88	1.32	0.36	0.72	1.08
Total Cost (\$M)	10.1	18.9	27.8	10.9	18	25.2
Payback time (years)	2	1	0.7	2.8	1.4	0.92
Break even (\$/kWh)	0.0354			0.0396		

Table 6.3: Cost Dish-Stirling systems in Lund

Cost Table: PV System, Lund					
CAPEX (\$M)	PV (\$M)	Battery (\$M)	Electricity (\$M/year)	Grid (\$M)	Total Cost (\$M)
9.9	5	8.8	0.13	0.5	17

Table 6.4: Specific costs of PV system in Lund

Table 6.3 shows that the initial investment cost (CAPEX) is significantly lower for both Dish-Stirling systems, the 33 unit system is of course lowest at \$M1.19 for SCIG and \$M1.24 for the DFIG, while the 99 unit system has a CAPEX \$3.57/3.73 and the PV system has a CAPEX of \$M9.9. Operational costs (OPEX) and total cost for the dish Stirling system are highly dependent on the gas price. The investment in more Dish-Stirling units reduces the operational costs, in the case of the SCIG system the increased investment does not pay off unless the gas price is quite high. The break even cost is the required gas cost to equalize the total cost of the PV system and the Dish-Stirling system. As can be seen in the table the 99 unit SCIG system actually requires a lower gas cost than the 33 unit system to break even. The 99 unit DFIG raises the break even cost by 12%. Investment in a DFIG system has a payback time of 0.7 - 2.8 years which is quite fast in the context of a total lifetime of 20 years.

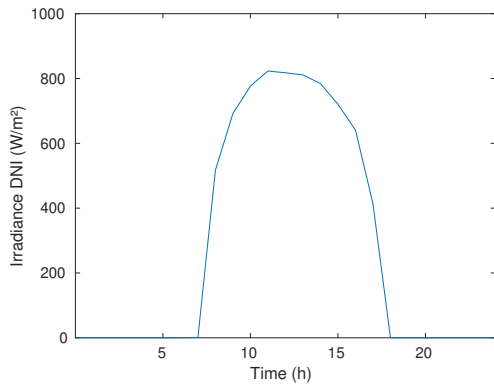
6.1.2 Location: Johannesburg, South Africa

Johannesburg has considerably better solar radiation conditions compared to Lund. The radiation levels are higher and remain consistently high over the whole year. This results in the PV system requiring less installed capacity in order to achieve the same power generation, the required solar panel area is also decreased to $25,500m^2$. However, a similar sized battery is required to service the night hours. The irradiation conditions allow the system to be designed to operate all year round. A grid connection is still installed in order to sell excess energy. The new PV specifications are presented in table 6.5.

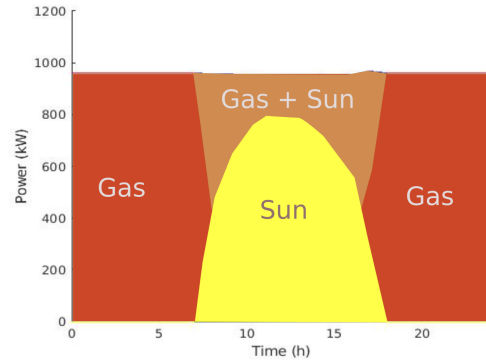
The Dish-Stirling systems are configured similarly as for the Lund location. The only difference is that the 99 unit systems will have a grid connection in order to sell excess electricity to the grid. The DNI profile (fig. 6.8a) offers significantly more solar energy than in Lund. Both the 33 unit system and the 99 unit system present significantly lower gas consumption over the whole year compared to Lund. This can also be observed in the energy mix pie-charts, figure 6.9a and 6.10a. The 99 unit systems will produce more energy than is used during the day, the excess is sold to the grid in order to offset the gas cost. Figure 6.10 shows that with these conditions regarding solar irradiation the difference for gas consumption between the 99 unit DFIG system and a SCIG system is less significant compared to Lund. The reason for that is that the incoming irradiation

PV	Value	Battery	Value
Installed capacity	5.1MWp	Size	14.7MWh
Module efficiency	20%	Round-trip efficiency	88%
System losses	14%	Lifetime	10 yrs
Mounting	Fixed	Technology	Li-ion

Table 6.5: Johannesburg PV system specifications



(a) Average DNI a day in July

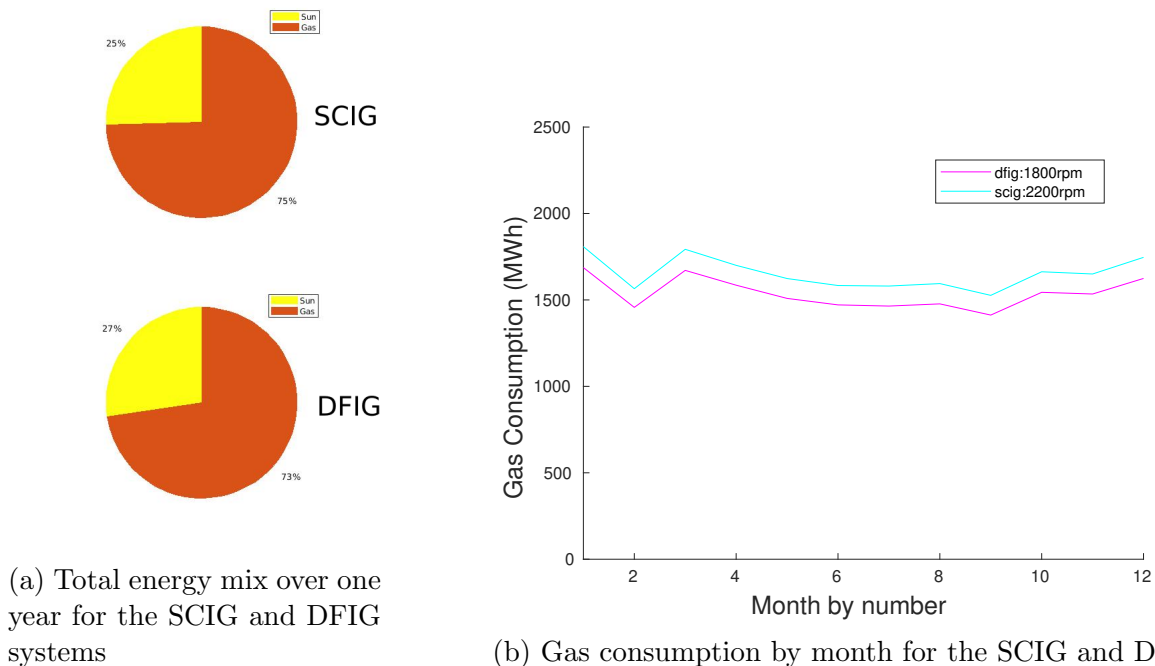


(b) Dish-Stirling hybrid power output for 33 unit DFIG system a day in July

Figure 6.8: Average DNI profile and Dish-Stirling power output, Johannesburg

tion is generally stronger in Johannesburg which allows both systems to reach the power demand during the day without the need of hybrid operation. During the night they both work at similar efficiency levels. However, the DFIG system is still more efficient at solar energy conversion and produce 9% more energy than the SCIG system. The 99 unit configuration also result in the Dish-Stirling systems producing more overall energy than the PV system as shown in figure 6.11b. This energy is sold to the grid and the income is used to offset the gas cost over the year. Similarly the excess energy generated by the PV system is sold to the grid.

The cost comparison in figure 6.12 shows similar results as for the installation in Lund. The Dish-Stirling system is cheaper after 20 years given that the fuel cost is low enough. The CAPEX is again significantly lower for the Dish-Stirling systems but not quite as



(a) Total energy mix over one year for the SCIG and DFIG systems

(b) Gas consumption by month for the SCIG and DFIG

Figure 6.9: Energy mix and gas consumption, 33 unit system, Johannesburg

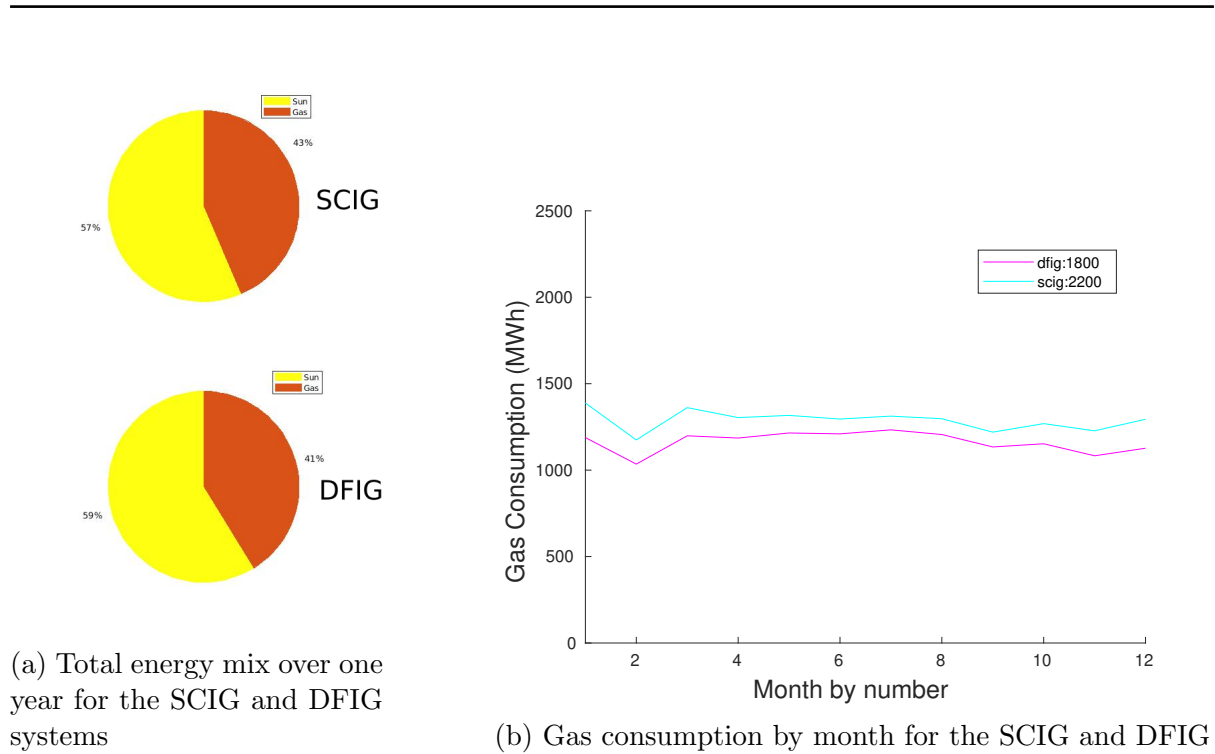


Figure 6.10: Energy mix and gas consumption, 99 unit system, Johannesburg

much as in Lund due to the lower PV capacity required. The DFIG system investment pays for itself in 0.6 - 2.9 years if excess energy is sold to the grid. The gas consumption difference between the DFIG and SCIG systems is not as large as in the Lund case, but the DFIG system still produces significantly more energy. By selling the excess energy to the grid operational costs are reduced. The gas consumption is lower in Johannesburg compared to Lund, however, the PV system performs better as well, making the break even gas price lower for the 33 unit systems. Investing in more Dish-Stirling units results in more solar power being utilized; this is shown to be beneficial regardless of the gas cost at this location. Both total cost and break even gas cost are better with the 99 unit systems. Due to the DFIG systems' superior performance with variable power input the 99 unit DFIG systems break even gas cost is significantly higher than the 99 unit SCIG

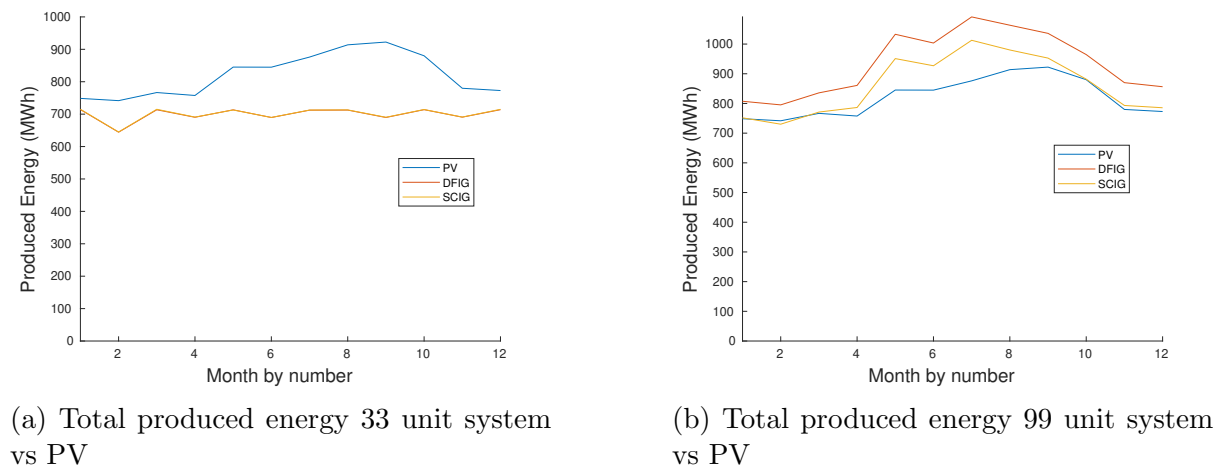
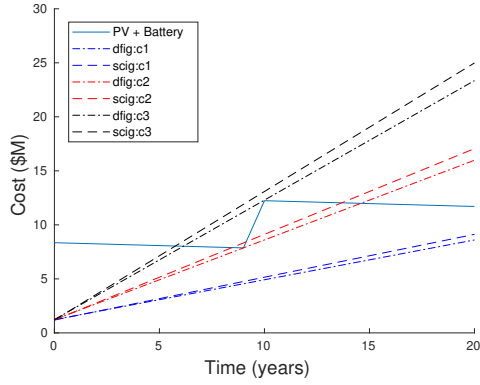
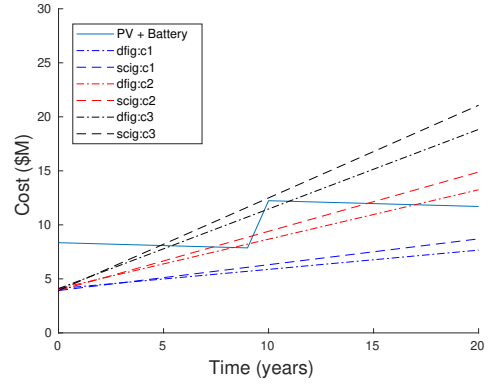


Figure 6.11: Total produced energy over one year, Johannesburg



(a) Cost over 20 years, 33 unit systems vs PV



(b) Cost over 20 years, 99 unit system vs PV

Figure 6.12: Project system cost over 20 years, Johannesburg. Three gas costs are considered: c1, c2, c3 which can be seen in table 6.2

system.

Cost Table: Johannesburg						
Cost	33 Unit System			99 Unit System		
Gas cost (\$/kWh)	0.02	0.04	0.06	0.02	0.04	0.06
SCIG						
CAPEX (\$/kWh)	1.19			3.92		
OPEX (\$M/year)	0.4	0.8	1.12	0.24	0.48	0.72
Total Cost (\$M)	9.1	17	25	8.7	14.9	21.1
Break even (\$/kWh)	0.0265			0.0297		
Electricity (\$M/year)	-			-0.07		
Grid (\$M)	-			0.392		
DFIG						
CAPEX (\$/kWh)	1.24			4.1		
OPEX (\$M/year)	0.37	0.74	1.11	0.18	0.32	0.54
Total Cost (\$M)	8.6	16	23.4	7.7	13.25	18.8
Payback time (years)	1.9	1	0.6	2.9	2	1.5
Break even (\$/kWh)	0.0284			0.0345		
Electricity (\$M/year)	-			-0.1		
Grid (\$M)	-			0.41		

Table 6.6: Cost Dish-Stirling systems Johannesburg

Cost Table: PV System					
CAPEX (\$M)	PV (\$M)	Battery (\$M)	Electricity (\$M/year)	Grid (\$M)	Total Cost (\$M)
8.35	3.57	8.84	-0.0535	0.357	11.7

Table 6.7: Specific costs for PV system Johannesburg

Chapter 7

Conclusions and Future Work

In this work a model of a Dish-Stirling system has been developed. Two different generator configurations have been modeled, studied and analyzed. The addition of an electrolyser to the system was modeled and control algorithms were developed to increase performance. Last, a comparative study between the proposed Dish-Stirling system and an equivalent PV based system has been conducted.

It has been shown that given a low enough gas price the Stirling hybrid system can be cheaper than a comparable PV and battery based system when electricity generation is considered. The main differences are that the PV and battery based system requires a large initial investment, both in economical terms and in consumed production energy. The PV system also requires 2.5-10 times more area compared to the proposed Dish-Stirling configurations. This is a result of the higher efficiency of the Dish-Stirling system and the fact that the PV system has to generate more energy in a shorter amount of time in the proposed configurations. If other technologies were introduced into the PV system these figures might be different but the results highlights the fact that the Hybrid Dish-Stirling technology is more flexible and self sufficient than PV technology. The Dish-Stirling system however needs a cheap and environmentally sound fuel source in order to be competitive. It is important to keep in mind that the Dish-Stirling system and PV system are not completely equivalent systems. The former system also produces thermal energy which holds almost twice as much energy as the produced electricity. If this energy could be harvested and used for e.g. district heating, it would provide a significant advantage for the Stirling solution. Additionally one of the main advantages of the Dish-Stirling system which is hard to quantify in monetary value is its flexibility. The fact that it can produce energy regardless of weather conditions can be extremely useful, especially in an energy system where a large part of the energy producing resources are intermittent, or in a scenario where there is a weak grid or no grid at all to rely on. The PV system can only supply energy during the dark hours if there was enough solar irradiation during the day. There are a lot of development opportunities regarding alternative heat sources and thermal storage in a Stirling based system as well.

The system comparison shows that the location of operation plays a big role in the performance. The Dish-Stirling system performs comparatively better in a location with lower solar insolation. The Dish-Stirling system consumes more fuel in this case but the PV system requires a high installed capacity and an additional energy source, like the power grid. At a location with higher consistent insolation all year round, investment in

more solar conversion capacity is beneficial. In the case of the Dish-Stirling system this means that investing in more dish units is more economical than using fewer units and more gas. It should be noted that all Dish-Stirling systems does not have to be hybrid capable in this scenario since most of the units only work with solar power, thus saving the cost of the corresponding gas burner in the initial investment.

The research shows that investing in a variable speed system configuration is most effective when the system works with varying power input, and especially at low power input. When the system was configured to work at constant maximum capacity the variable speed was simply not used, however the higher energy extraction of the DFIG proved very beneficial. This shows that even a few percent increased efficiency translates to considerable cost savings down the line. More research should be made to identify the most efficient system configuration in regards to generator type, speed and pressure at a constant power level conversion scenario. When the system works solely on solar power, the variable speed configuration was considerably more effective than the fixed speed configuration. The systems simulated in this work have neither been optimized nor validated against an actual Dish-Stirling system. The model accounts for engine efficiency corresponding to engine pressure but according to Martini [13] the engine rotational speed also has a major effect on efficiency. Future work should focus examining this correlation experimentally in order to be able to make the model more accurate and reliable.

The ability to control the power quality of the generated power can be critical when generating power connected to a local energy system. In section 5.2 it was shown that an APF would require a similar amount of power converter capacity as the DFIG system. If reactive power compensation is required, the DFIG system has a big advantage as no additional investment is needed. If the cost estimation is accurate the additional investment cost for the DFIG system would be around \$25/kW. However, if a power consumer, like an electrolyser, is connected to the DC-link the conditions change slightly. The APF in the SCIG system will not require a big increase in converter capacity due to the relation of active and reactive power flowing through the converter. The DFIG GSC capacity on the other hand needs to be increased significantly unless the load is only operated in specific scenarios. When the system operates at super-synchronous speeds the rotor power flow can be fed into the load. It is possible to imagine a system with increased RSC converter capacity that could feed more rotor power to a load than the current configuration. This would in turn reduce the capacity requirement for the GSC and at the same time allow the generator to operate at higher rotational speeds. Consideration needs to be taken to what the operational conditions and benefits of such a system would be.

Bibliography

- [1] Dolf Gielen and Francisco Boshell. “The role of renewable energy in the global energy transformation”. In: *Energy Strategie Reviews* 24 (2019), pp. 38–50.
- [2] Anthony Wang and van der Leun Kees. *European Hydrogen Backbone*. Report. Guidhouse, 2020.
- [3] Hassan Farhangi. “The path of the smart grid”. In: *IEEE Power and Energy Magazine* 8.11024473 (2010), pp. 18–28.
- [4] Mehmet Rida Tur and Ramazan Bayindir. “A Review of Active Power and Frequency Control in Smart Grid”. In: Global Power, Energy and Communication Conference. 1. 2019.
- [5] Vinnova. *Electric Farm*. URL: <https://www.vinnova.se/en/p/electric-farm/>. (accessed: 04.07.2020).
- [6] K.W. Stone and H.W. Braun. “Stirling Energy Systems (SES) dish-Stirling program”. In: IECEC-97 Proceedings of the Thirty-Second Intersociety Energy Conversion Engineering Conference. 5920214. IEEE, 1997.
- [7] DOE/Sandia National Laboratories. *Solar Power: New World Record For Solar-to-grid Conversion Efficiency Set*. URL: www.sciencedaily.com/releases/2008/02/080213172955.htm. (accessed: 10.08.2020).
- [8] Jeff Shepard. *NTR plc To Invest \$100 Million In Solar Firm Stirling Energy Systems*. URL: <https://eepower.com/news/ntr-plc-to-invest-100-million-in-solar-firm-stirling-energy-systems/#>. (accessed: 10.08.2020).
- [9] Eric Wesoff. *Stirling Energy Systems, Dish-Engine Solar Maker, Files for Chapter 7 Bankruptcy*. URL: www.greentechmedia.com/articles/read/stirling-energy-systems-dish-engine-solar-maker-files-for-chapter-7-bankrup. (accessed: 10.08.2020).
- [10] ENERGY.GOV. *Crystalline Silicon Photovoltaics Research*. URL: <https://www.energy.gov/eere/solar/crystalline-silicon-photovoltaics-research>. (accessed: 30.11.2020).
- [11] Theocharis Tsoutsos and Niki Frantzeskaki. “Environmental impacts from the solar energy technologies”. In: *Energy Policy* 33 (2005), pp. 289–296.
- [12] Raghava Kommalapati and Akhil Kadiyala. “Review of the Life Cycle Greenhouse Gas Emissions from Different Photovoltaic and Concentrating Solar Power Electricity Generation Systems”. In: *Energies* 10.350 (2017).
- [13] W R Martini. *Stirling engine design manual. Second edition*. U.S. DEPARTMENT OF ENERGY Conservation, Renewable Energy Office of Vehicle, and Engine RD, Jan. 1983.

-
- [14] Charles W. Lopez and Kenneth W. Stone. *Performance of the Southern California Edison Company Stirling Dish*. Report. Mako Enterprises Southern California Edison Company PO Box 800 Rosemead, California 91770: Sandia National Laboratories, 1993.
- [15] Mats Alaküla, Per Karlsson, and Hans Bängtsson. *Power Electronics: Devices, Converters, Control and Applications*. Lund University, 2019.
- [16] Mohit Bajaj and Amit Kumar Singh. “Grid integrated renewable DG systems: A review of power quality challenges and state-of-the-art mitigation techniques”. In: *International Journal of Energy Research* 44.1 (2020), pp. 26–69. eprint: <https://onlinelibrary.wiley.com/doi/pdf/10.1002/er.4847>. URL: <https://onlinelibrary.wiley.com/doi/abs/10.1002/er.4847>.
- [17] Alireza Khaligh and Omer C. Onar. “23 - Energy Sources”. In: *Power Electronics Handbook (Fourth Edition)*. Ed. by Muhammad H. Rashid. Fourth Edition. Butterworth-Heinemann, 2018, pp. 725–765. ISBN: 978-0-12-811407-0. DOI: <https://doi.org/10.1016/B978-0-12-811407-0.00025-8>. URL: <https://www.sciencedirect.com/science/article/pii/B9780128114070000258>.
- [18] S. Joshi and Prof. Dr. V.J.Pandya. “A Brief Survey on Wind Energy Conversion Systems Modeling of PMBLDCG based Wind Turbine”. In: *National Conference on Power Electronics Systems Applications, PESA*. 2013.
- [19] A. Beainy and N. Moubayed C. Maatouk. “Comparison of Different Types of Generator for Wind Energy Conversion System Topologies”. In: (2016).
- [20] Abu Dhabi. *Innovation landscape brief: Utility-scale Batteries*. Report. International Renewable Energy Agency, 2019.
- [21] Erik Emilsson and Lisbeth Dahllöf. *Lithium-Ion Vehicle Battery Production, Status 2019 on Energy Use, CO2 Emissions, Use of Metals, Products Environmental Footprint, and Recycling*. Report. IVL Swedish Environmental Research, 2019.
- [22] Kendall Mongird and Vilayanur Viswanathan. *2020 Grid Energy Storage Technology Cost and Performance Assessment*. Report. U.S Department of Energy, 2020.
- [23] Souleman N. Motapon, Enric Lachance, Louis-a. Dessanint, et al. “Generic Cycle Life Model for Lithium-Ion Batteries Based on Fatigue Theory and Equivalent Cycle Counting”. In: *Solar Energy Materials Solar Cells* 95.11024473 (2011), pp. 3359–3369.
- [24] Sameer Khare and Mark Dell’Amico. “Selection of materials for high temperature latent heat energy storage”. In: *Solar Energy Materials Solar Cells* 107 (2012), pp. 0927–0248.
- [25] Jens F. Peters and Manuel Baumann. “The environmental impact of Li-Ion batteries and the role of keyparameters—A review”. In: *Renewable and Sustainable Energy Reviews* 67 (2017), pp. 491–506.
- [26] O. Schmidt and A. Gambhir. “Future cost and performance of water electrolysis: An expert elicitation study”. In: *International journal of hydrogen energy* 42 (), pp. 30479–30492.
- [27] Dr. Z. Sun and S. W. Koh. “Solar-Driven Alkaline Water Electrolysis with Multifunctional Catalysts”. In: *Advanced Functional Materials* 30 (), pp. 2002138–2002147.

-
- [28] *IEEE Application Guide for IEEE Std 1547, IEEE Standard for Interconnecting Distributed Resources with Electric Power Systems*. 2009.
- [29] Victor F. Mendes and Guilherme M. Rezende. “25kW DFIG Wind Energy Conversion System Prototype for Voltage Sag Tests”. In: *Anais do V Simpósio Brasileiro de Sistemas Elétricos*. 2014.
- [30] Richard Gagnon. *Wind Farm - DFIG Average Model*.
- [31] Michael A. Snyder. *Development of Simplified Models of Doubly-Fed Induction Generators (DFIG)*. Göteborg, Sweden, 2012.
- [32] Dr John Fletcher and Jin Yang. *Introduction to the Doubly-Fed Induction Generator for Wind Power Applications, Paths to Sustainable Energy*. 2010.
- [33] Alfredo Ursa and Pablo Sanchis. “Static-dynamic modelling of the electrical behaviour of a commercial advanced alkaline water electrolyser”. In: *International journal of hydrogen energy* 37 (), pp. 18598–18614.
- [34] Thomas Huld, Gabi Friesen, Artur Skoczek, et al. “A power-rating model for crystalline silicon PV modules”. In: *Solar Energy Materials Solar Cells* 95.11024473 (2011), pp. 3359–3369.
- [35] PHOTOVOLTAIC GEOGRAPHICAL INFORMATION SYSTEM. *Crystalline Silicon Photovoltaics Research*. URL: https://re.jrc.ec.europa.eu/pvg_tools/en/#MR. (accessed: 05.02.2021).
- [36] Arnulf JÄGER-WALDAU. *PV Status Report 2019*. Report. European Commission, 2019.
- [37] Henk Polinder, Frank F. A. van der Pijl, Gert-Jan de Vilder, et al. “Comparison of Direct-Drive and Geared Generator Concepts for Wind Turbines”. In: *IEEE TRANSACTIONS ON ENERGY CONVERSION* 21 (2006), pp. 725–733.

Appendix A

Electrolyzer Equations

ΔH = Enthalpy change of process

ΔG = Gibbs energy

Q = Thermal energy

T = Temperature

ΔS = Entropy change

z = Electron moles exchanged to produce one mole of hydrogen

F = Faraday's constant

V_{rev}^0 = Reversible voltage as a function of temperature at 1(bar) pressure

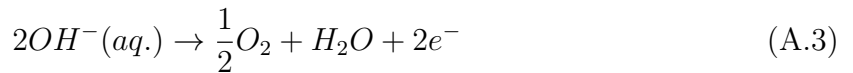
$P_{v,KOH}$ = Vapor pressure (bar)

$a_{H_2O,KOH}$ = water activity (aw)

P_{V,H_2O} = vapour pressure of pure water (bar)

R = Gas constant ($\text{kgm}^2 \text{K}^{-1} \text{mol}^{-1} \text{s}^{-2}$)

The basic process of electrolysis and its half reactions are represented as:



The total enthalpy change of the process (ΔH) determines the amount of energy needed to start the process. The total enthalpy of the process depends on two parts: the Gibbs energy (ΔG) and the thermal energy Q , the thermal energy is equal to the product of temperature (T) and entropy change ΔS resulting in the equation:

$$\Delta G = \Delta H - Q = \Delta H - T\Delta S \quad (\text{A.4})$$

Gibbs energy can be expressed in voltage as:

$$V_{rev} = \frac{\Delta G}{zF} \quad (\text{A.5})$$

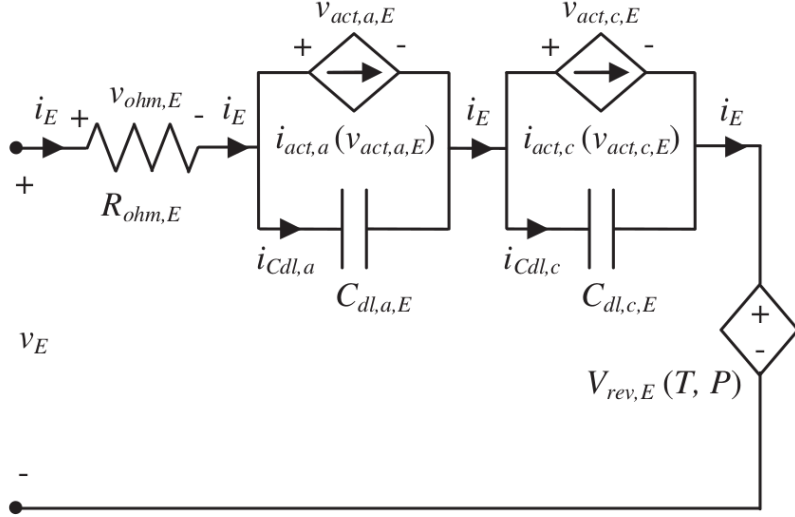


Figure A.1: Static-Dynamic model of alkaline electrolyser [33]

V_{rev} is the minimum ideal voltage required to induce electrolysis. The cell voltage V_{cell} is given as V_{rev} plus some voltages related to irreversibilities:

$$V_{cell} = V_{rev} + V_{act} + V_{ohm} \quad (\text{A.6})$$

Where V_{act} is related to activation electrochemical kinematics of the anode and cathode. This is very non linear and follows a logarithmic profile dependent on the current through the cell. V_{ohm} is related to resistive energy loss.

$V_{rev,E}$ is the ideal reversible voltage of the entire cell stack with N_s number of cells.

$$V_{rev,E} = N_s V_{rev} = N_s \left[V_{rev,T}^0 + \frac{R(T + 273.15)}{zF} \ln \left(\frac{(P - P_{v,KOH})(P - P_{v,KOH})^{1/2}}{a_{H_2O,KOH}} \right) \right] \quad (\text{A.7})$$

The $V_{rev,E}$ term is dependent on two terms the first dependent on temperature and the second on pressure. $V_{rev,T}^0$ is the reversible voltage dependent on temperature at a constant pressure of 1 bar. The second is an expression dependent on pressure and includes some non-ideal conditions due to vapor pressure P_{v,H_2O} and the water activity (wa)

$$V_{rev,T}^0 = 1.5184 - 1.5421 \times 10^{-3}(T + 273.15) + 9.526 \times 10^{-5}(T + 273.15) \ln(T + 273.15) + 9.84 \times 10^{-8}(T + 273.15)$$

$$P_{v,KOH} = \exp(2.3202a + b \ln(P_{v,H_2O})) \quad (\text{A.8})$$

$$a = -0,0151m - 1.6788 \times 10^{-3}m^2 + 2.2588 \times 10^5m^3 \quad (\text{A.9})$$

$$b = 1 - 1.2062 \times 10^{-3}m + 5.6024 \times 10^{-4}m^2 - 7.8228 \times 10^{-6}m^3 \quad (\text{A.10})$$

$$P_{v,H_2O} = \exp\left(81.6179 - \frac{7699.68}{(T + 273.15)} - 10.9 \ln(T + 273.15) + 9.5891 \times 10^{-3}(T + 273.15)\right) \quad (\text{A.11})$$

$$a_{H_2O,KOH} = \exp\left(-0.05192m + 0.003302m^2 + \frac{3.177m - 2.131m^2}{T + (273.5)}\right) \quad (\text{A.12})$$

In order to simulate the dynamic properties of the electrolyzer the activation phenomena needs to be considered. The model of the activation phenomena consists of a current source dependent on the activation voltage in parallel with a double layered capacitor (fig. A.1). Activation voltage for cathode and anode are given by the following equations.

$$v_{act,a,E} = N_s v_{act,a} = N_s s \ln\left(\frac{1}{t} i_{act,a} + 1\right) \rightarrow i_{act,a} = t \left(e^{\frac{v_{act,a,E}}{N_s s}} - 1\right) \quad (\text{A.13})$$

$$v_{act,c,E} = N_s v_{act,c} = N_s s \ln\left(\frac{1}{w} i_{act,c} + 1\right) \rightarrow i_{act,c} = w \left(e^{\frac{v_{act,c,E}}{N_s s}} - 1\right) \quad (\text{A.14})$$

The temperature dependent constants: s , t , w and v are hardware specific and depends on the electrolyser that is uses. They are given by the I-V relationship of the actual machine and are acquired experimentally. In this project it is assumed that the electrolyser used is of a very similar design to the one presented in the paper that this model is based [33]. The constants are therefore assigned according to the results presented in that work.

$$s = s_1 + s_2 T + s_3 T^2 \quad (\text{A.15})$$

$$w = w_1 + w_2 T + w_3 T^2 \quad (\text{A.16})$$

$$t = t_1 + t_2 T + t_3 T^2 \quad (\text{A.17})$$

$$v = v_1 + v_2 T + v_3 T^2 \quad (\text{A.18})$$

The voltage drop dependent on resistance is dependent on the cross sectional area of the cell A_{cell} and and a temperature dependent constant r .

$$R_{ohm,E} = N_s R_{ohm} = N_s \frac{r}{A_{cell}} \quad (\text{A.19})$$

$$r = r_1 + r_2 T + \frac{r_3}{T} + \frac{r_4}{T^2} \quad (\text{A.20})$$